Philosophical Magazine
Publication details, including instructions for authors and subscription information:
http://www.tandfonline.com/loi/tphm20

The maximal advance path constraint for the homogenization of materials with random network microstructure

Mykola Tkachuk [a] & Christian Linder [a]

[a] Institute of Applied Mechanics (CE), Chair I, University of Stuttgart, Pfaffenwaldring 7, 70550 Stuttgart, Germany

Available online: 30 Apr 2012

To cite this article: Mykola Tkachuk & Christian Linder (2012): The maximal advance path constraint for the homogenization of materials with random network microstructure, Philosophical Magazine, DOI:10.1080/14786435.2012.675090

To link to this article: http://dx.doi.org/10.1080/14786435.2012.675090

Philosophical Magazine
2012, 1–30, iFirst

The maximal advance path constraint for the homogenization of materials with random network microstructure

Mykola Tkachuk and Christian Linder*

Institute of Applied Mechanics (CE), Chair I, University of Stuttgart, Pfaffenwaldring 7, 70550 Stuttgart, Germany

(*Received 20 December 2011; final version received 2 March 2012*)

This paper presents a non-affine homogenization scheme for materials with a random network microstructure. It is based on a newly developed kinematic constraint that links the microscopic deformation of the network to the macroscopic strain of the material. This relation accounts for the network functionality and is established by means of maximal advance paths that are long enough to reach the macroscopic scales of the continuous body and deform accordingly but are also composed of the microscopic fibres that follow the network deformation. The exact distribution of the variable fibre stretch is determined by the principle of minimum averaged free energy, which ultimately allows one to derive the homogenized elastic response of the network at equilibrium. Besides the general formulation, the model is presented in detail for the case of tetrafunctional networks, for which the micro–macro relation and the expression for the homogenized elastic stress are derived in a compact and interpretable tensorial form. The performance of the model as well as the convexity and stability of the obtained homogenized response of the material is examined for networks composed of two different types of fibres, namely flexible chains and stiff filaments. The qualitative behaviour of the networks predicted for the two considered cases agrees with experimentally observed phenomena for soft materials. This includes a consistent explanation for the difference in the stiffness of elastomers at uniaxial and equibiaxial extension as well as a validation of recent experimental investigations of atypical normal stress amplitudes in biopolymer gels under shear loading.

Keywords: random networks; micromechanics; homogenization; soft matter; elastomers; biopolymers

1. Introduction

Network microstructures are commonly encountered in materials of artificial as well as natural origin. Elastomers [1], hydrogels and soft biological tissues [2–4], non-woven fabrics [5,6], and cellular foams [7] are all on the microscopic level composed of elongated one-dimensional elements one can generally address as fibres. When these soft materials are subject to a macroscopic strain, the underlying microstructure undergoes a peculiar deformation. The forces produced by the deformed

*Corresponding author. Email: linder@mechbau.uni-stuttgart.de

ISSN 1478–6435 print/ISSN 1478–6443 online

http://dx.doi.org/10.1080/14786435.2012.675090
http://www.tandfonline.com

Table 1. Overview of random network models.

Refs.	Geometry	Kinematics	Microdeformation
Discrete models			
[8–13]	Randomly generated discrete network of fibres	Stretch and bending of fibres by the corresponding degrees of freedom	Generic network deformation as a result of statical or thermodynamical equilibrium
Network average models			
[14–17]	Statistical distribution of fibre geometry in the network	Axial stretch of fibres from this distribution	Affine deformation of the microstretch distributions
[22–25]	Eight fibres placed on the diagonals of a rectangular box	Identical axial stretch of these eight fibres	The rectangular box deforms with principal stretches
[20,27]	Isotropic distribution of fibre orientations	Axial stretch as a function of the initial orientation	Non-affine microstretch minimizing the averaged energy

filaments and their interaction within the irregular three-dimensional network constitute the macroscopic stress response of the material. The knowledge about the micromechanics of random networks is therefore crucial for the understanding of mechanical properties like elasticity displayed by the above-mentioned soft materials.

Their networks are essentially discrete mechanical systems, where single fibres are the basic structural units. The existing theories and models of random networks in the literature can be categorized as done in Table 1. The first category includes the discrete models that reproduce the microstructure in detail. Such an approach allows one to examine networks of different nature and capture the effect of various specific phenomena such as the entropic and enthalpic response of fibres to axial straining and their instant bending [8–10], initial internal stresses [11,12], or thermal fluctuations of network junctions [13]. The network simulations provide deep insight into the microscopic mechanisms of the macroscopic response produced by these soft materials. Nevertheless, they often require an enormous computational effort and produce results that display statistic scattering which is different from one generated random network to another.

The alternative class of models discussed in Table 1 is based on the mean field approach for the description of random networks. They are commonly used to constitute the material response of continuous solids in finite element simulations. These theories treat the large microscopic networks in terms of average distributions instead of resolving them in detail. In particular, the considered statistical quantities describe the microdeformation of the network. Their relation to the macroscopic strain, which is the main external action on the material, is the key question addressed by these mean field models in different ways. The most obvious assumption is that the microdeformation and the mean quantities defining it change affinely with the deformation gradient of the solid. This can be quite commonly observed in the classical models for rubber elasticity [14,15] as well as for

more recent works on semiflexible networks [16,17]. Comparison to the experimental data [18] as well as the results of discrete network simulations [9,10] indicate though that the affine assumption is not universally valid. It does not explain numerous phenomena known for soft matter which are attributed to the non-affine character of the microdeformation. In this work two of them are addressed. These are the difference in the locking strain for uniaxial and equibiaxial loadings of elastomers composed of flexible chains with limiting extensibility [18–20] as well as the transition from the soft bending dominated to the stiffened stretching dominated response of dilute biological gels composed of semiflexible filaments [9–11,21]. In reality the non-affinity comes from both, the peculiar response of fibres and their interaction in the network which is commonly highly non-linear, and the complex kinematics of the networks described by the internal degrees of freedom. The latter issue, the adequate representation of the network microdeformation, is a central point for the development of micromechanically based models of soft matter.

Several non-affine models have so far been developed to resolve this issue. The eight-chain model proposed in [22] for rubber-like elastomers and later adopted for other materials [23–25] postulates the distribution of stretch identical to the stretch of eight particularly aligned filaments. In the seminal work [20], the non-affine microsphere model suggests certain variations of stretch constrained by a specific relation to the macroscopic deformation with the exact distribution of stretch determined by the principle of minimal free energy. A similar approach can be found in the analytical model of [26] with respect to the principle of maximal entropy. The two latter models introduce a concept of the relaxing variable microdeformation that is subject to the kinematic constraints of the macroscopic strain. A different way to introduce non-affinity can be found in [27] where a phenomenological compliance stretch is considered. The concept is in good agreement with the nature of the elastic response produced by the microstructure of a solid at equilibrium. Nevertheless, the already existing non-affine network models of this type can be improved by replacing the often artificial design of the micro–macro relation with a physical-based relation.

In this work we propose a new micromechanically justified construction of the kinematic constraints based on the formalism of *maximal advance paths* in the network. These paths allow one to perform the transition between the microscopic scale of single fibres to the macroscopic scale of the deforming continuous solid. These constraints result in an efficient homogenization scheme inspired by the orientation-based approach proposed in [20] which is characterized by a well interpretable expression of the homogenized stress in terms of the microscopic fibre forces.

The paper is organized as follows. In Section 2, the statistical description of the network and its microdeformation is introduced. Section 3 is devoted to the formulation of *the maximal advance path constraint* for an arbitrary functionality of the network which is the main contribution of this work. Next, a particular case of tetrafunctional networks is chosen and treated in more detail to illustrate the performance of the proposed model. Section 4 concerns the relaxation of the microstretch in the network governed by the principle of the minimum averaged free energy and the derivation of the homogenized elastic response of the material at equilibrium. Finally, the performance of the model is investigated in Section 5 for two qualitatively different types of fibre response in the form of flexible chains as

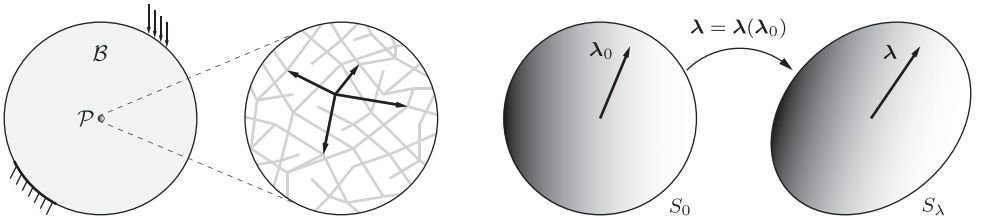

Figure 1. The random network microstructure of a continuous solid $\mathcal{B}$ at a material point $\mathcal{P}$ (on the left) formed by long fibres (straight lines) with the end-to-end vectors plotted at one of the junctions (black arrows). Statistical description of a random network (on the right) as an assembly of fibres with initial isotropic orientations $\boldsymbol{\lambda}_0$ uniformly distributed on a unit sphere S_0 and the network deformation defined by the microstretch vector function $\boldsymbol{\lambda}(\boldsymbol{\lambda}_0)$: $\boldsymbol{\lambda}_0 \in S_0 \mapsto \boldsymbol{\lambda} \in S_\lambda \subset \mathbb{R}^3$.

well as stiff filaments. The predicted non-affine deformation in networks comprised of such fibres allows one to explain the difference in stiffening of elastomers under uniaxial and equibiaxial extension as well as the atypical stress responses recently observed in experiments on biopolymer gels. Section 6 gives a summary to the presented results and elaborates on possible future extensions of the approach.

2. Statistical description of random networks

Microscopic networks considered in this work have an irregular three-dimensional structure. They are formed by a large number of fibres connected together at junction points. Since one of their dimensions dominates over the others, these fibres can be considered essentially as one-dimensional entities as displayed in Figure 1.

Following the motivation given in the introductory Section 1, this work is based on the statistical approach to the treatment of random networks. Within this approach individual fibres are not treated separately but are included into a statistical assembly in which they are differentiated by certain key attributes. In particular, the statistical description proposed in this section classifies the fibres of the network by their initial orientation in the undeformed state similar to [20,28]. The deformation of the network is correspondingly not determined by the deformation of single fibres but by the distribution of the deformation parameters over the introduced assembly of fibres. The network total quantities such as the elastic energy are then consistently derived by distribution averaging. This formalism naturally provides the homogenization of random network microstructures.

The proposed statistical description is based on the following assumptions about the network composition, geometry and deformation:

(1) junction points do not perform any thermal motion, hence they do take certain positions in space;
(2) all the fibres in the network are of one single type and have uniform properties (equal molecular weight, contour length, stiffness etc.);
(3) in the initial network configuration all the fibres have the same end-to-end distance R_0 and are oriented isotropically in all the directions;
(4) the deformation of fibres with equal initial orientation coincides strictly.

With these assumptions, the identification of the network with the assembly of fibres distinguished only by their initial orientation is justified.

Without loss of generality it can be assumed that in the initial configuration all the fibres have a unit stretch $|\boldsymbol{\lambda}_0| = 1$ where the initial stretch vector $\boldsymbol{\lambda}_0 = \boldsymbol{R}_0/R_0$ is the end-to-end vector $\boldsymbol{R}_0$ scaled by the initial end-to-end distance R_0. The dimensionless stretch vector is preferred over the end-to-end vector for the characterization of the fibre microdeformation. This allows one to avoid an otherwise needed account of the length R_0 of the fibres which is uniform in the network. Therefore, $\boldsymbol{\lambda}_0$ is a unit vector representing the initial orientation of the fibres by which they are distinguished in the undeformed network. The assembly of all the fibres can furthermore be associated with a unit sphere S_0, each point on the sphere corresponding to a certain fibre orientation $\boldsymbol{\lambda}_0$ as shown in Figure 1. Since all the fibres initially are assumed to be equally distributed in all the directions, or correspondingly over the unit sphere S_0, the orientation density function scaled by the factor $1/|S_0| = 1/(4\pi)$ has a uniform unit value in the undeformed state, namely $p_0(\boldsymbol{\lambda}_0) = 1$. This function expresses the fraction of fibres in the network with an initial orientation in the infinitesimal vicinity $\mathrm{d}\boldsymbol{\lambda}_0$ of $\boldsymbol{\lambda}_0$ as

$$\frac{1}{|S_0|} p_0(\boldsymbol{\lambda}_0) |\mathrm{d}\boldsymbol{\lambda}_0| = \frac{1}{|S_0|} |\mathrm{d}\boldsymbol{\lambda}_0|. \tag{1}$$

The averaging over the network of an arbitrary quantity $\zeta = \zeta(\boldsymbol{\lambda}_0)$ which depends on the initial fibre orientation is then performed by means of the surface integral

$$\langle \zeta \rangle = \frac{1}{|S_0|} \int_{S_0} \zeta(\boldsymbol{\lambda}_0) |\mathrm{d}\boldsymbol{\lambda}_0|. \tag{2}$$

The deformation of the network within the proposed formalism is described by a vector-valued function $\boldsymbol{\lambda}(\boldsymbol{\lambda}_0)$. Its value is the microstretch vector defined as $\boldsymbol{\lambda} = \boldsymbol{R}/R_0$ where $\boldsymbol{R}$ is the end-to-end vector of the deformed fibres with reference orientation $\boldsymbol{\lambda}_0$. This function maps the microsphere S_0 into $\mathbb{R}^3$ or more particularly, provided the function $\boldsymbol{\lambda}(\boldsymbol{\lambda}_0)$ is continuous, onto a stretch surface S_λ as shown in Figure 1 based on

$$\boldsymbol{\lambda}(\boldsymbol{\lambda}_0) \colon \boldsymbol{\lambda}_0 \in S_0 \mapsto \boldsymbol{\lambda} \in S_\lambda \subset \mathbb{R}^3. \tag{3}$$

In the deformed state the averaging of a stretch dependent quantity $\zeta = \zeta(\boldsymbol{\lambda})$ is performed similar to (2) as

$$\langle \zeta \rangle = \frac{1}{|S_0|} \int_{S_0} \zeta(\boldsymbol{\lambda}(\boldsymbol{\lambda}_0)) |\mathrm{d}\boldsymbol{\lambda}_0|. \tag{4}$$

The proposed statistical description contains the most essential information about the network and its deformation which is provided by the stretch vector function. This is essential for the development of the model presented in this work. Other orientation-based network models operate with scalar fields such as the absolute value of the fibre stretch [20,27], the orientation density function [28,29], or the end-to-end vector distribution density [26,30], which is less informative. As an exception, the microsphere-based model [31] incorporates a variable vector field, although this is different to the one presented in this work. It does not describe the actual stretch of the fibres but their referential reorientation due to the remodeling of

a soft tissue. In this work the evolution of the fibre stretch vector represents the two main deformation mechanisms in the network: the axial straining of fibres and their reorientation. The response of fibres to the axial stretch is used to constitute the homogenized elastic properties of the material in Section 4. Still, as introduced so far the distribution of the microstretch is arbitrary. Its relation to the macroscopic deformation is established by a special kinematic constraint derived in the next section.

***Remark 1*:**

(1) Only half of the microsphere matters for the above network characterization, since there is no essential difference between the orientations $\boldsymbol{\lambda}_0$ and $-\boldsymbol{\lambda}_0$. To not favour one particular hemisphere it is assumed that the fibres are equally divided between opposite directions.
(2) To preserve the intrinsic central symmetry of the stretch vector distribution within the proposed statistical description, the map (3) has to satisfy the condition $\boldsymbol{\lambda}(-\boldsymbol{\lambda}_0) = -\boldsymbol{\lambda}(\boldsymbol{\lambda}_0)$.
(3) The developed model deals with finite material strains as well as large fibre deformations and correspondingly is set up within the non-linear geometry framework. Nevertheless, the tensorial derivations performed in this work are for simplicity presented with respect to orthonormal cartesian coordinates. Hence, metric tensors are overall omitted.

3. The maximal advance path constraint

In this work, *network paths* are considered to formulate the constraints relating the microdeformation of the network to the macrodeformation of the continuum body. These paths are formed by the fibres connecting the junctions of the network. As long as the network is static, like in the case of elasticity, these paths remain unbroken during deformation. A path, consisting of i microscopic fibres with stretch vectors $\boldsymbol{\lambda}_i$, can connect points of the body at a distance above the microscale of the network, hence ascending to the scale of the macroscopic continuum. The path is though still restricted to the material point level so that the overall deformation is characterized by the deformation gradient $\boldsymbol{F}$. This allows one to establish the connection between the network scales and the material point scales linking the microdeformation to the macrodeformation.

In particular, specific paths that have the maximal advance in a certain direction, called *maximal advance paths*, are considered in this work. They are defined in the initial undeformed configuration of the network where all the chains have unit stretch and are oriented equally in all directions. Let $\boldsymbol{l}_0$ with $|\boldsymbol{l}_0| = 1$ be a certain direction of interest. Then the advance of a fibre with orientation $\boldsymbol{\lambda}_0$ along $\boldsymbol{l}_0$ is

$$\xi = \boldsymbol{\lambda}_0 \cdot \boldsymbol{l}_0. \tag{5}$$

The cumulative distribution function for this random scalar variable is

$$\mathcal{F}_\xi(x) = P(\xi = \boldsymbol{\lambda}_0 \cdot \boldsymbol{l}_0 \leqslant x) = \frac{1}{|S_0|} \int_{S_{0,x}} |\mathrm{d}\boldsymbol{\lambda}_0| = \frac{x+1}{2}, \tag{6}$$

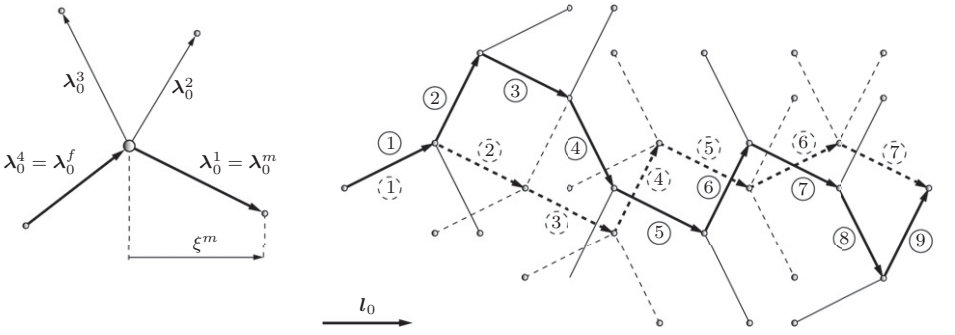

Figure 2. The maximal advance path constraint. Illustration of a cross-link belonging to a path and the chain with maximal advance ξ^m along the direction $\boldsymbol{l}_0$ on the left. Illustration of the effect of functionality f on the straightness of the path on the right where two networks with $f=3$ (solid lines) and $f=4$ (additional segments plotted in dashed lines) and the two resulting maximal advance paths are shown. The higher the functionality, the straighter the paths become.

where $S_{0,x} = \{\boldsymbol{\lambda}_0 \in S_0 \colon \boldsymbol{\lambda}_0 \cdot \boldsymbol{l}_0 \leqslant x\}$ is the subset of orientations in which the advance in direction $\boldsymbol{l}_0$ is lesser than or equal to x. The corresponding probability density function is then computed as

$$p_\xi(x) = \frac{\mathrm{d}}{\mathrm{d}x}\mathcal{F}_\xi(x) = \frac{1}{2}. \tag{7}$$

Consider now a junction which belongs to a maximal advance path schematically illustrated in Figure 2. It is connected to f fibres with initial orientations $\{\boldsymbol{\lambda}_0^i\}_{i=1}^f$, where f is the functionality of the network. Provided the path has come to the junction by the fibre $\boldsymbol{\lambda}_0^f$, there will be $f-1$ remaining fibres along which it may propagate further. These fibres have orientation vectors $\{\boldsymbol{\lambda}_0^i\}_{i=1}^{f-1}$, being random variables distributed uniformly over the unit sphere S_0 and are assumed to be non-correlating. The advance in the direction $\boldsymbol{l}_0$ along these fibres is given by $f-1$ random variables $\xi^i = \boldsymbol{\lambda}_0^i \cdot \boldsymbol{l}_0$, each having the distribution (6). The maximal advance from the junction in the direction $\boldsymbol{l}_0$ is then given by

$$\xi^m = \max\{\xi^i\}_{i=1}^{f-1}, \tag{8}$$

which is a random quantity characterized by the cumulative distribution function

$$\mathcal{F}_{\xi^m}(x) = P\left(\xi^m = \max\{\xi^i\}_{i=1}^{f-1} \leqslant x\right) = \prod_{i=1}^{f-1} P(\xi^i \leqslant x) = \left(\frac{x+1}{2}\right)^{f-1} \tag{9}$$

and the corresponding probability density function

$$p_{\xi^m} = \frac{f-1}{2}\left(\frac{x+1}{2}\right)^{f-2}. \tag{10}$$

Whereas the average advance in the network $\langle\xi\rangle = 0$, the average maximal advance

$$\langle\xi^m\rangle = \int_{-1}^{1} x\,\mathrm{d}\mathcal{F}_{\xi^m}(x) = \frac{f-2}{f} \tag{11}$$

is non-zero. In addition to the value of the maximal advance ξ^m it is important to know by which fibre it is attained. Let $\boldsymbol{\lambda}_0^m = \arg\max\{\boldsymbol{\lambda}_0 \cdot \boldsymbol{l}_0, \boldsymbol{\lambda}_0 \in \{\boldsymbol{\lambda}_0^i\}_{i=1}^{f-1}\}$ be the fibre with the maximal advance in the direction $\boldsymbol{l}_0$ and belong to the path. Then it has a distribution

$$p^m(\boldsymbol{\lambda}_0, \boldsymbol{l}_0) = (f-1)\left(\frac{\boldsymbol{\lambda}_0 \cdot \boldsymbol{l}_0 + 1}{2}\right)^{f-2}, \tag{12}$$

which is radially symmetric on the unit sphere of orientations S_0 relative to the $\boldsymbol{l}_0$ axis. It represents the assembly of fibres $\boldsymbol{\lambda}_0^m$ in the maximal advance path in the direction $\boldsymbol{l}_0$ and has the property

$$\langle \boldsymbol{\lambda}_0^m \rangle = \frac{1}{|S_0|}\int_{S_0} \boldsymbol{\lambda}_0 p^m(\boldsymbol{\lambda}_0, \boldsymbol{l}_0)|\mathrm{d}\boldsymbol{\lambda}_0| = \frac{f-2}{f}\boldsymbol{l}_0. \tag{13}$$

The end-to-end vector $\boldsymbol{R}_{l_0}$ of a long maximal advance path composed of n_{l_0} fibres, where n_{l_0} is large, is then given by

$$\boldsymbol{R}_{l_0} = n_{l_0}\langle R_0 \boldsymbol{\lambda}_0^m \rangle = n_{l_0} R_0 \frac{f-2}{f}\boldsymbol{l}_0 \tag{14}$$

in terms of the average of the orientation vector in the path (13). Once the length of such a path is large enough it becomes a macroscopic object. Correspondingly, one can expect that with the macroscopic deformation its end-to-end vector will change affinely following the deformation gradient map $\boldsymbol{F}$, i.e.

$$\boldsymbol{R}_l = \boldsymbol{F}\boldsymbol{R}_{l_0} = n_{l_0} R_0 \frac{f-2}{f}\boldsymbol{l} \quad \text{where } \boldsymbol{l} = \boldsymbol{F}\boldsymbol{l}_0. \tag{15}$$

On the other hand this deformed path is composed of the deformed fibres $\boldsymbol{\lambda}^m = \boldsymbol{\lambda}(\boldsymbol{\lambda}_0^m)$ from the assembly (12) and $\boldsymbol{R}_l$ is alternatively given by the path average

$$\boldsymbol{R}_l = n_{l_0}\langle R_0 \boldsymbol{\lambda}^m \rangle. \tag{16}$$

Matching (15) and (16), one obtains for all path directions $\boldsymbol{l}_0$ the relation

$$\boxed{\langle \boldsymbol{\lambda}^m \rangle = \frac{f-2}{f}\boldsymbol{l} \;\sim\; \frac{1}{|S_0|}\int_{S_0} \boldsymbol{\lambda}(\boldsymbol{\lambda}_0) p^m(\boldsymbol{\lambda}_0, \boldsymbol{l}_0)|\mathrm{d}\boldsymbol{\lambda}_0| = \frac{f-2}{f}\boldsymbol{F}\boldsymbol{l}_0,} \tag{17}$$

which provides, since $\boldsymbol{l}_0 \in S_0$, an infinite set of constraints to the variable microscopic deformation field $\boldsymbol{\lambda}(\boldsymbol{\lambda}_0)$. The derived constraint (17) is denoted as the *maximal advance path constraint* (MAPC).

At least one microdeformation will always satisfy the constraint, namely the affine stretch $\bar{\boldsymbol{\lambda}}(\boldsymbol{\lambda}_0) = \boldsymbol{F}\boldsymbol{\lambda}_0$. In case all the fibres $\boldsymbol{\lambda}_0^m$ in the path deform affinely as $\bar{\boldsymbol{\lambda}}^m = \boldsymbol{F}\boldsymbol{\lambda}_0^m$ the path itself will also undergo an affine deformation

$$\langle \bar{\boldsymbol{\lambda}}^m \rangle = \boldsymbol{F}\langle \boldsymbol{\lambda}_0^m \rangle \;\sim\; \frac{1}{|S_0|}\int_{S_0} \bar{\boldsymbol{\lambda}}(\boldsymbol{\lambda}_0) p^m(\boldsymbol{\lambda}_0, \boldsymbol{l}_0)|\mathrm{d}\boldsymbol{\lambda}_0| = \frac{f-2}{f}\boldsymbol{F}\boldsymbol{l}_0. \tag{18}$$

The *full affine network models* (FANM) [15,28] postulate that the networks strictly follow this microdeformation in response to the macroscopic strain disregarding the nature of fibres in the network. In contrast, the proposed approach in this work

suggests that $\bar{\boldsymbol{\lambda}}$ is just one of the many other variations of the microstretch kinematically compatible with the macroscopic deformation. The response of the affine network is later compared to the alternative behaviour predicted by the proposed model in Section 5.

The micro–macro relation (17) takes the form of a linear 1-type Fredholm integral equation and depends on the function $\boldsymbol{\lambda}(\boldsymbol{\lambda}_0)$ which has an essential property of negative symmetry as pointed out in Remark 1. Therefore only its values in one hemisphere of orientations matter so that the average of the fibre stretch vector in the deformed path can be alternatively written as

$$\langle \boldsymbol{\lambda}^m \rangle = \frac{1}{|S_0|} \int_{S_0} \boldsymbol{\lambda}(\boldsymbol{\lambda}_0) \tilde{p}^m(\boldsymbol{\lambda}_0, \boldsymbol{l}_0) |\mathrm{d}\boldsymbol{\lambda}_0| \tag{19}$$

where $\tilde{p}^m(\boldsymbol{\lambda}_0, \boldsymbol{l}_0) = \frac{1}{2}[p^m(\boldsymbol{\lambda}_0, \boldsymbol{l}_0) - p^m(-\boldsymbol{\lambda}_0, \boldsymbol{l}_0)]$. Since $\tilde{p}^m(\boldsymbol{\lambda}_0, -\boldsymbol{l}_0) = -\tilde{p}^m(\boldsymbol{\lambda}_0, \boldsymbol{l}_0)$, another property of the assembly average is

$$\langle \boldsymbol{\lambda}^m \rangle|_{\boldsymbol{l}_0 = -\boldsymbol{l}_0} = \frac{1}{|S_0|} \int_{S_0} \boldsymbol{\lambda}(\boldsymbol{\lambda}_0) \tilde{p}^m(\boldsymbol{\lambda}_0, -\boldsymbol{l}_0) |\mathrm{d}\boldsymbol{\lambda}_0| = -\langle \boldsymbol{\lambda}^m \rangle. \tag{20}$$

As long as the right-hand side of (17) is an odd function of $\boldsymbol{l}_0$ it is sufficient that the equality is satisfied for path directions $\boldsymbol{l}_0$ spanning only half of the orientation space, i.e. the constraint (17) is a Fredholm type equation on a hemisphere $S_0^{1/2}$:

$$\boxed{\begin{gathered} \frac{1}{|S_0|} \int_{S_0} \boldsymbol{\lambda}(\boldsymbol{\lambda}_0) \tilde{p}^m(\boldsymbol{\lambda}_0, \boldsymbol{l}_0) |\mathrm{d}\boldsymbol{\lambda}_0| = \frac{f-2}{f} \boldsymbol{F}\boldsymbol{l}_0 \quad \forall \boldsymbol{l}_0 \in S_0^{1/2} \\ \text{with } \boldsymbol{\lambda}\colon S_0^{1/2} \to \mathbb{R}^3, \quad \boldsymbol{\lambda}(-\boldsymbol{\lambda}_0) = -\boldsymbol{\lambda}(\boldsymbol{\lambda}_0), \quad \tilde{p}^m(\boldsymbol{\lambda}_0, \boldsymbol{l}_0)\colon S_0^{1/2} \times S_0^{1/2} \to \mathbb{R} \end{gathered}} \tag{21}$$

A closer examination of the kernel function $\tilde{p}^m(\boldsymbol{\lambda}_0, \boldsymbol{l}_0)$ of the Fredholm integral operator in (21) reveals that it is a polynomial for the natural values of the network functionality $f \in \mathbb{N}$. It can be written as a finite series expansion

$$\tilde{p}^m(\boldsymbol{\lambda}_0, \boldsymbol{l}_0) = \sum_{\alpha} \phi_\alpha(\boldsymbol{\lambda}_0) \psi_\alpha(\boldsymbol{l}_0), \tag{22}$$

where $\alpha \in \{1, \ldots, a\} = \mathcal{A}$ and $\{\phi_\alpha(\boldsymbol{\lambda}_0)\}_{\alpha=1}^a$ and $\{\psi_\alpha(\boldsymbol{l}_0)\}_{\alpha=1}^a$ are linearly independent so that the Fredholm integral operator has a finite rank and its image is a linear combination of $\{\psi_\alpha(\boldsymbol{l}_0)\}_{\alpha=1}^a$.

As long as the affine stretch satisfies the maximal advance path constraint (18), the integral equation (21) can be rewritten in a homogeneous form

$$\frac{1}{|S_0|} \int_{S_0} \big[\boldsymbol{\lambda}(\boldsymbol{\lambda}_0) - \bar{\boldsymbol{\lambda}}(\boldsymbol{\lambda}_0)\big] \tilde{p}^m(\boldsymbol{\lambda}_0, \boldsymbol{l}_0) |\mathrm{d}\boldsymbol{\lambda}_0| = \boldsymbol{0} \tag{23}$$

in terms of the difference of the microstretch $\boldsymbol{\lambda}$ and the affine stretch $\bar{\boldsymbol{\lambda}}$. Using the series expansion (22), one can further derive

$$\sum_{\alpha=1}^{a} \left\{ \frac{1}{|S_0|} \int_{S_0} \big[\boldsymbol{\lambda}(\boldsymbol{\lambda}_0) - \bar{\boldsymbol{\lambda}}(\boldsymbol{\lambda}_0)\big] \phi_\alpha(\boldsymbol{\lambda}_0) |\mathrm{d}\boldsymbol{\lambda}_0| \right\} \psi_\alpha(\boldsymbol{l}_0) = \boldsymbol{0} \quad \forall\, \boldsymbol{l}_0 \in S_0. \tag{24}$$

Due to the linear independence of $\{\psi_\alpha(\boldsymbol{l}_0)\}_{\alpha=1}^{a}$, (24) is satisfied if and only if

$$\frac{1}{|S_0|}\int_{S_0}\left[\boldsymbol{\lambda}(\boldsymbol{\lambda}_0)-\bar{\boldsymbol{\lambda}}(\boldsymbol{\lambda}_0)\right]\phi_\alpha(\boldsymbol{\lambda}_0)|\mathrm{d}\boldsymbol{\lambda}_0|=\boldsymbol{0}\quad\forall\alpha\in\mathcal{A} \tag{25}$$

so that the maximal advance path constraint (21) is essentially equivalent to a finite set of constraints (25).

For an illustrative purpose the detailed presentation of the maximal advance path constraint and the resulting homogenization scheme in the remaining part of this work is limited to networks of functionality $f=4$. Firstly, such networks are most typical for vulcanized rubbers and biopolymers [32]. Secondly, for this value of functionality the proposed micro–macro constraint takes a very particular intuitive form. The average maximal advance (11) in the undeformed configuration takes with $f=4$ the value $\langle\xi^m\rangle=1/2$. This means that the maximal advance paths in tetrafunctional networks are quite far from being straight. Correspondingly, one can expect an essential non-affinity due to the potential stretch redistribution which is subject to the constraint (21). To obtain the equivalent finite set of constraints (25), consider the particular expression the kernel $\tilde{p}^m$ takes for $f=4$, i.e.

$$\tilde{p}^m(\boldsymbol{\lambda}_0,\boldsymbol{l}_0)=\frac{1}{2}\left[3\left(\frac{\boldsymbol{\lambda}_0\cdot\boldsymbol{l}_0+1}{2}\right)^2-3\left(\frac{-\boldsymbol{\lambda}_0\cdot\boldsymbol{l}_0+1}{2}\right)^2\right]=\frac{3}{2}\boldsymbol{\lambda}_0\cdot\boldsymbol{l}_0, \tag{26}$$

which is a polynomial in terms of cartesian coordinates of the initial orientation vector $\boldsymbol{\lambda}_0=[x_0,y_0,z_0]$ and the path direction vector $\boldsymbol{l}_0=[\tilde{x}_0,\tilde{y}_0,\tilde{z}_0]$ with $\boldsymbol{\lambda}_0\cdot\boldsymbol{l}_0=x_0\tilde{x}_0+y_0\tilde{y}_0+z_0\tilde{z}_0$. The kernel can be written in the form of the series expansion (22) with

$$\left\{\phi_\alpha(\boldsymbol{\lambda}_0)\right\}_{\alpha=1}^{3}=\left\{x_0,y_0,z_0\right\}\quad\text{and}\quad\left\{\psi_\alpha(\boldsymbol{l}_0)\right\}_{\alpha=1}^{3}=\left\{\frac{3}{2}\tilde{x}_0,\frac{3}{2}\tilde{y}_0,\frac{3}{2}\tilde{z}_0\right\}. \tag{27}$$

With the particular set of linearly independent $\left\{\phi_\alpha(\boldsymbol{\lambda}_0)\right\}_{\alpha=1}^{3}$ given in (27) the three vectorial constraints (25) can be represented in the following tensorial form

$$\frac{1}{|S_0|}\int_{S_0}\left[\boldsymbol{\lambda}(\boldsymbol{\lambda}_0)-\bar{\boldsymbol{\lambda}}(\boldsymbol{\lambda}_0)\right]\otimes\boldsymbol{\lambda}_0|\mathrm{d}\boldsymbol{\lambda}_0|=\boldsymbol{0}. \tag{28}$$

The average of the dyadic product $\langle\bar{\boldsymbol{\lambda}}\otimes\boldsymbol{\lambda}_0\rangle$ can be easily found as

$$\frac{1}{|S_0|}\int_{S_0}\bar{\boldsymbol{\lambda}}(\boldsymbol{\lambda}_0)\otimes\boldsymbol{\lambda}_0|\mathrm{d}\boldsymbol{\lambda}_0|=\boldsymbol{F}\cdot\frac{1}{|S_0|}\int_{S_0}\boldsymbol{\lambda}_0\otimes\boldsymbol{\lambda}_0|\mathrm{d}\boldsymbol{\lambda}_0|=\frac{1}{3}\boldsymbol{F} \tag{29}$$

with the help of the identity $\langle\boldsymbol{\lambda}_0\otimes\boldsymbol{\lambda}_0\rangle=\frac{1}{3}\boldsymbol{1}$. This ultimately allows one to obtain the formulation of the maximal advance path constraint for *tetrafunctional* networks in the form

$$\frac{1}{|S_0|}\int_{S_0}\boldsymbol{\lambda}(\boldsymbol{\lambda}_0)\otimes\boldsymbol{\lambda}_0|\mathrm{d}\boldsymbol{\lambda}_0|=\frac{1}{3}\boldsymbol{F}, \tag{30}$$

which appears to be very natural. Indeed, the term $\boldsymbol{\lambda}\otimes\boldsymbol{\lambda}_0$ in a certain way represents the deformation of a single fibre, as it maps the initial unit orientation vector $\boldsymbol{\lambda}_0$ of

the fibre onto the fibre stretch vector $\boldsymbol{\lambda}$. Correspondingly, (30) can be viewed as the relation between the averaged network microdeformation and the local macroscopic deformation represented by $\boldsymbol{F}$.

To conclude, this section gives the general formulation of the maximal advance path constraint (21). It relates the microdeformation of the network described within the statistical representation introduced in Section 2 to the local macroscopic deformation of the material. It is shown that for a given functionality f of the network only a finite set of constraints (25) is imposed onto the microstretch $\boldsymbol{\lambda}(\boldsymbol{\lambda}_0)$. The functionality included in the formulation of the constraints is a very important characteristic of the network topology. Its qualitative influence on the kinematics of the network is discussed in the section and the remarks below. Ultimately, for the case of $f=4$, to which the remaining part of this work corresponds, the maximal advance path constraint is derived in the particular tensorial form (30).

***Remark 2*:**

(1) The higher the functionality of the network the larger and closer to 1 is the value of the average maximal advance (11) due to the availability of straighter paths in networks with a greater number of fibres at each junction.
(2) An increased functionality f of the network results in an increase of the number of the degree of the polynomial (22) as well as an increase of independent constraints (25) on the microstretch $\boldsymbol{\lambda}$. Correspondingly, for higher values of the network functionality one will observe a smaller deviation from the affine stretches $\bar{\boldsymbol{\lambda}}$ in the network. This agrees with the above remark on the straightness of the maximal advance path. In a path which is too straight there is almost no place for stretch redistribution.
(3) Although the set (27) makes use of a particular orthonormal coordinate system in the reference configuration it is invariant to coordinate transformation. That is if one performs a coordinate transformation $\boldsymbol{Q}$: $[x_0, y_0, z_0] \rightarrow [x_0', y_0', z_0']$ the set (27) can be restored in its particular form by a linear recombination.

4. Network relaxation and homogenized response at equilibrium

The maximal advance path constraint formulated in the previous section does not define the microstretch $\boldsymbol{\lambda}$ but only restricts its variation at a given macroscopic strain. To constitute ultimately the microdeformation of the network, the principle of minimum free energy is used in this work. It states that within all the kinematically possible microdeformations the fibres will deform so that the total network energy is minimized. This approach was initially proposed in [20] for the formulation of the non-affine microsphere model of rubber elasticity, which establishes a general homogenization scheme adopted in this work to incorporate the kinematic micro–macro relation developed in the previous section. The elastic response of the network retrieved by this principle can be viewed as a result of microstructure relaxation by the internal degrees of freedom. The latter are statistically represented by the fibre stretch function $\boldsymbol{\lambda}(\boldsymbol{\lambda}_0)$ as described in Section 2.

The statistical representation of the network microdeformation exploited so far contains only information about the stretch of the fibres. Consequently, within the proposed approach one can only consider the situation in which the free energy allows for an expression in terms of the fibre stretch. In particular, this can certainly be done in the case when the networks are composed of fibres that only interact at the junctions and themselves have a free energy that simply changes with the axial strain. Unentangled networks of flexible polymer molecules in some swollen and dry elastomers as well as semiflexible biopolymer networks and networks with stiff mechanical filaments fit well into this category.

As long as the energy originates from separate fibres the network total energy Ψ_{net} can be generally computed by the sum of energy contributions $\psi_f(|\boldsymbol{\lambda}|)$ of all its fibres, which can be expressed in terms of the network average as

$$\Psi_{\text{net}}[\boldsymbol{\lambda}] = n\langle\psi_f(|\boldsymbol{\lambda}|)\rangle. \tag{31}$$

Here n is the initial network density expressing the number of fibres in the unit volume of the undeformed material, to which also the homogenized free energy Ψ_{net} is referred. With respect to the given form of the network energy in (31) one can specifically address the variational principle stated above as the *minimum averaged free energy principle*. Its mathematical formulation restricted to the central case of tetrafunctional networks with $f=4$ is based on the tensorial version of the maximal advance path constraint (30) and reads as:

$$\boxed{\begin{aligned}\Psi_{\text{net}}[\boldsymbol{\lambda}] \sim \langle\psi_f\rangle &= \frac{1}{|S_0|}\int_{S_0}\psi_f(|\boldsymbol{\lambda}(\boldsymbol{\lambda}_0)|)|\mathrm{d}\boldsymbol{\lambda}_0| \underset{\boldsymbol{\lambda}(\boldsymbol{\lambda}_0)}{\longrightarrow} \min\\ \langle\boldsymbol{\lambda}\otimes\boldsymbol{\lambda}_0\rangle &= \frac{1}{|S_0|}\int_{S_0}\boldsymbol{\lambda}(\boldsymbol{\lambda}_0)\otimes\boldsymbol{\lambda}_0|\mathrm{d}\boldsymbol{\lambda}_0| = \frac{1}{3}\boldsymbol{F}.\end{aligned}} \tag{32}$$

The fibre energy ψ_f is assumed to be a convex, continuous and differentiable function of $|\boldsymbol{\lambda}|$. By the first assumption fibre instabilities are excluded from consideration. The second one guarantees that the functional $\Psi_{\text{net}}[\boldsymbol{\lambda}]$ or the average fibre energy $\langle\psi_f\rangle$, when defined, are differentiable with respect to the microstretch function $\boldsymbol{\lambda}$. There are some further properties of ψ_f that define whether the constrained minimization problem (32) is well-posed. These are discussed in the next section with respect to two practically important types of fibre responses. So far the existence and uniqueness of a stretch solution $\boldsymbol{\lambda}^*$ is postulated for a yet unspecified set of deformations $\mathfrak{F}$. The minimizing stretch can be, correspondingly, viewed as a function $\boldsymbol{\lambda}^* = \boldsymbol{\lambda}^*(\boldsymbol{F})$ of the deformation gradient $\boldsymbol{F}\in\mathfrak{F}\subset \mathrm{SO}(3)$.

In the remaining part of this section the properties of the equilibrium microdeformation of the network and its relaxed homogenized response resulting from (32) are examined. For this purpose consider the Lagrangian of the constrained minimization problem (32) which can be written as

$$L[\boldsymbol{\lambda}, \mathbf{v}] = \frac{1}{|S_0|}\int_{S_0}\psi_f(|\boldsymbol{\lambda}(\boldsymbol{\lambda}_0)|)|\mathrm{d}\boldsymbol{\lambda}_0| - \mathbf{v}\colon\left(\frac{1}{|S_0|}\int_{S_0}\boldsymbol{\lambda}(\boldsymbol{\lambda}_0)\otimes\boldsymbol{\lambda}_0|\mathrm{d}\boldsymbol{\lambda}_0| - \frac{1}{3}\boldsymbol{F}\right), \tag{33}$$

where $\mathbf{v}$ is the second-order tensor of Lagrange multipliers, as long as the micro–macro constraint (30) is tensorial for the considered case of tetrafunctional networks.

The Euler–Lagrange equation enforces the vanishing variation of L with the microstretch $\boldsymbol{\lambda}$ at $\boldsymbol{\lambda}^*$. The stationarity condition gives the relation

$$\boldsymbol{f}_f^* = f_f(|\boldsymbol{\lambda}^*|)\frac{\boldsymbol{\lambda}^*}{|\boldsymbol{\lambda}^*|} = \boldsymbol{\nu}\boldsymbol{\lambda}_0, \tag{34}$$

where $\boldsymbol{f}_f = \partial\psi_f/\partial\boldsymbol{\lambda}$ is the stretch conjugate fibre force which relaxes towards $\boldsymbol{f}_f^* = \boldsymbol{f}_f(\boldsymbol{\lambda}^*)$ at equilibrium and $f_f = \partial\psi_f/\partial|\boldsymbol{\lambda}|$ is its magnitude proportional to the actual fibre force $F_f = \partial\psi_f/\partial|\boldsymbol{R}|$.

Once the equilibrium microstretch response $\boldsymbol{\lambda}^*$ is known for any admissible deformation $\boldsymbol{F} \in \mathfrak{F}$ the homogenized properties of the material can be determined. In particular, one can find the change of the total free energy of the relaxed network with the variable macroscopic deformation

$$\Psi_{\text{net}}^*(\boldsymbol{F}) = n\langle\psi_f(|\boldsymbol{\lambda}^*|)\rangle = \frac{1}{|S_0|}\int_{S_0}\psi_f(|\boldsymbol{\lambda}^*|)|\mathrm{d}\boldsymbol{\lambda}_0|. \tag{35}$$

Furthermore, the homogenized mechanical stress can be obtained by the standard reasoning of thermodynamics [33] as the derivative of the free energy with respect to the strain field. The derivation in the deformation gradient results in the first Piola–Kirchhoff stress tensor computed as

$$\boldsymbol{P} = \partial_{\boldsymbol{F}}\Psi_{\text{net}}^* = n\langle\partial_{\boldsymbol{F}}\psi_f(|\boldsymbol{\lambda}^*|)\rangle = n\frac{1}{|S_0|}\int_{S_0}\boldsymbol{f}_f^*\cdot\frac{\partial\boldsymbol{\lambda}^*}{\partial\boldsymbol{F}}|\mathrm{d}\boldsymbol{\lambda}_0|. \tag{36}$$

The integral on the right-hand side of this equation can be further transformed into the sum

$$\frac{1}{|S_0|}\int_{S_0}\boldsymbol{f}_f^*\cdot\frac{\partial\bar{\boldsymbol{\lambda}}}{\partial\boldsymbol{F}}|\mathrm{d}\boldsymbol{\lambda}_0| + \frac{1}{|S_0|}\int_{S_0}\boldsymbol{f}_f^*\cdot\frac{\partial(\boldsymbol{\lambda}^*-\bar{\boldsymbol{\lambda}})}{\partial\boldsymbol{F}}|\mathrm{d}\boldsymbol{\lambda}_0| \tag{37}$$

in which the second term is identically zero. To prove this claim, note that the constraint in the form (28) is invariantly satisfied by the equilibrium stretch $\boldsymbol{\lambda}^*$ for all $\boldsymbol{F}$ so that

$$\langle(\boldsymbol{\lambda}^*-\bar{\boldsymbol{\lambda}})\otimes\boldsymbol{\lambda}_0\rangle \equiv 0 \quad\Rightarrow\quad \langle\partial_{\boldsymbol{F}}(\boldsymbol{\lambda}^*-\bar{\boldsymbol{\lambda}})\otimes\boldsymbol{\lambda}_0\rangle \equiv 0. \tag{38}$$

Contracting this identity with the tensor $\boldsymbol{\nu}$ of Lagrange multipliers yields the equation

$$\frac{1}{|S_0|}\int_{S_0}(\boldsymbol{\nu}\boldsymbol{\lambda}_0)\cdot\frac{\partial(\boldsymbol{\lambda}^*-\bar{\boldsymbol{\lambda}})}{\partial\boldsymbol{F}}|\mathrm{d}\boldsymbol{\lambda}_0| = \boldsymbol{0} \tag{39}$$

in which the left-hand side can be identified as the second integral in (37) using the relation (34). With the help of the identity $\partial_{\boldsymbol{F}}\bar{\boldsymbol{\lambda}} = \boldsymbol{1}\otimes\boldsymbol{\lambda}_0$ the remaining part of the expression gives the elastic stress in the form

$$\boldsymbol{P} = n\frac{1}{|S_0|}\int_{S_0}\boldsymbol{f}_f^*\otimes\boldsymbol{\lambda}_0|\mathrm{d}\boldsymbol{\lambda}_0| = n\langle\boldsymbol{f}_f^*\otimes\boldsymbol{\lambda}_0\rangle \tag{40}$$

in terms of fibre forces in the relaxed network. Again, just as the constraint (30) the stress is obtained in a very natural form. Similar expressions are generally derived for

continuous bodies in which the stress is transmitted by microscopic axial forces [34]. This, in particular, indicates that the statistical description of the microdeformation proposed in Section 2 and the maximal advance path constraint developed in Section 3 together adequately represent the kinematics of the network and the continuous solid. With the expression (34) for the fibre force vector $\boldsymbol{f}_f^*$, the first Piola–Kirchhoff stress tensor can be alternatively derived in a compact way as

$$\boldsymbol{P} = n\langle(\mathbf{v}\boldsymbol{\lambda}_0) \otimes \boldsymbol{\lambda}_0\rangle = \frac{1}{3} n\mathbf{v}, \tag{41}$$

which establishes the stress-like nature of the Lagrange multiplier tensor $\mathbf{v}$.

It is again emphasized that the obtained particular results are derived in this section for the tetrafunctional networks with $f=4$ for which the micro–macro constraint is given by (30) and the energy related to fibre straining is given by (31). Nevertheless the proposed homogenization approach can be easily extended to networks of arbitrary functionality with a free energy other than the one in (31). Firstly, one can make use of the more general form of the micro–macro relation (25) in the case of $f \neq 4$. Secondly, the variational principle stated in this section is universal and not limited to a particular expression of the free energy.

As concerns the particular model developed in this section, it allows for an efficient numerical implementation by means of a unit sphere discretization and quadrature formulas proposed in [35]. The numerical results illustrating the performance of the proposed approach are given next in Section 5 where the non-affine network response is examined qualitatively for two different types of fibres.

5. Predicted non-affine microdeformation of flexible and stiff networks

Within the proposed approach the elastic response of soft materials with random microstructures is related to the relaxation of internal degrees of freedom in the network subject to the constraint of the macroscopic deformation. The statistical description of the fibre stretch in the network, the maximal advance path constraint that relates it to the local deformation gradient of the material, and the principle of the averaged free energy that finally constitutes the equilibrium microdeformation are most generally presented in the previous sections. For tetrafunctional networks composed of fibres that only respond to the axial straining the tensorial constraint (30) and the identity (34) for the stretch and force vectors of the fibres at equilibrium, as well as the expression for the homogenized mechanical stress (40) are derived. The presented results are so far obtained for fibres of arbitrary nature, the only assumption taken about their free energy ψ_f is that it can be expressed as a convex, continuous and differentiable function of the stretch vector $|\boldsymbol{\lambda}|$. In this section two particular cases corresponding to two qualitatively different types of fibres are examined in more detail.

The distinction is made with respect to the absolute value of the stretch at which the minimum of the fibre free energy is attained. Some flexible fibres have the free energy with a minimum at zero end-to-end distance. The response of such fibres is primarily entropic and their zero stretch corresponds to the most probable configuration. Such behaviour is typical of flexible polymer chains with the

persistence length much smaller than the length of the chain between the adjacent junctions [32]. In the opposite case the fibres are stiff and have the minimal free energy at non-zero elongation. Such response is displayed either by semiflexible biopolymer molecules or by stiff mechanical filaments and corresponds to the limit when the persistence length is comparable or much larger than the fibre dimensions [36]. The network response differs qualitatively for the two considered cases, which altogether cover a broad class of materials [6]. Therefore, the investigation given below is of high relevance.

The main subjects that this examination addresses are the existence and uniqueness of the equilibrium microstretch as the solution to the constrained minimization problem (32) as well as the stability of the homogenized material. Furthermore, the peculiar properties of the non-affine networks predicted by the proposed model are discussed based on their correspondence with experimentally observed phenomena.

5.1. *MAPC predicted non-affine deformation in networks of flexible chains*

A free energy with the minimum at zero end-to-end distance is predicted for flexible chains by several models of highest importance for polymer mechanics. Though being a result of idealization, it applies to many real polymer molecules that constitute natural and synthetic elastomers and biogels. With a certain degree of approximation such molecules are viewed as chains of segments that are either freely connected or rotating around the bonds, or, alternatively, can change their orientation relative to the adjacent segments for an enthalpic cost that is small compared to $k_{\mathrm{B}}T$. The latter quantity given in terms of k_{B}, the Boltzmann's constant, and T, the temperature, is the characteristic kinetic energy of thermal fluctuations. The response to the change of the end-to-end distance $R=|\boldsymbol{R}|$ produced by such chains is mainly entropic and is in particular described by *the Gaussian chain* [37,38], *the non-Gaussian freely rotating chain* [14] and *the worm-like chain* [39] models developed within the framework of statistical mechanics. These three mentioned models are summarized in Table 2, which contains the particular expressions for their free energy, and their chain force is plotted qualitatively in Figure 3.

In this subsection the microdeformation of networks made of such flexible chains is examined within the proposed homogenization approach. The uniqueness of the equilibrium microstretch is in general proved for this case. It is furthermore shown that the resulting homogenized network stress is stable at finite strains in the case of material incompressibility. The two particular above-mentioned chain models, namely the linear Gaussian chain and the nonlinear Langevin chain, are considered in detail. It is shown for the latter case that the microstretch in the network becomes substantially non-affine as chains approach their limiting extensibility. This effect explains qualitatively the character of stress stiffening observed in elastomers at uniaxial and biaxial tension.

To begin with the proof of uniqueness, note first that the models of flexible thermally fluctuating chains in common predict a free energy that is always a monotone convex function of the end-to-end distance $|\boldsymbol{R}|$ or equivalently the stretch $|\boldsymbol{\lambda}|$ as well as the positive entropic force that increases with straining starting with a

Table 2. Flexible chain models.

Model	Free energy ψ_f	Thermodynamic force F_f
Gaussian chain[a]	$\frac{3}{2}k_{\mathrm{B}}T\frac{R^2}{Nb^2}$	$3k_{\mathrm{B}}T\frac{R}{Nb^2}$
Freely rotating chain[a,b]	$Nk_{\mathrm{B}}T\left(\lambda_r\mathcal{L}^{-1}(\lambda_r)+\ln\frac{\mathcal{L}^{-1}(\lambda_r)}{\sinh\mathcal{L}^{-1}(\lambda_r)}\right)$	$k_{\mathrm{B}}T\frac{1}{b}\mathcal{L}^{-1}(\lambda_r)$
Worm-like chain[c]	$\frac{k_{\mathrm{B}}T}{4l_p}\frac{R^2}{L}\left[2+\frac{1}{1-R/L}\right]$	$\frac{k_{\mathrm{B}}T}{4l_p}\left[4\frac{R}{L}+\frac{1}{(1-R/L)^2}-1\right]$

Notes: [a]N is the number of chain segments, b is the Kuhn segment length.
[b]$\lambda_r = R/L$ is the relative stretch with $L = Nb$ being the contour length of the chain, $\mathcal{L}^{-1}$ is the inverse to the Langevin function $\mathcal{L}(\cdot) = \coth(\cdot) - 1/(\cdot)$.
[c]Given is the approximation of [40] valid in the limit $l_p \ll L$ where l_p is the persistence length of the worm-like chain and L is its contour length.

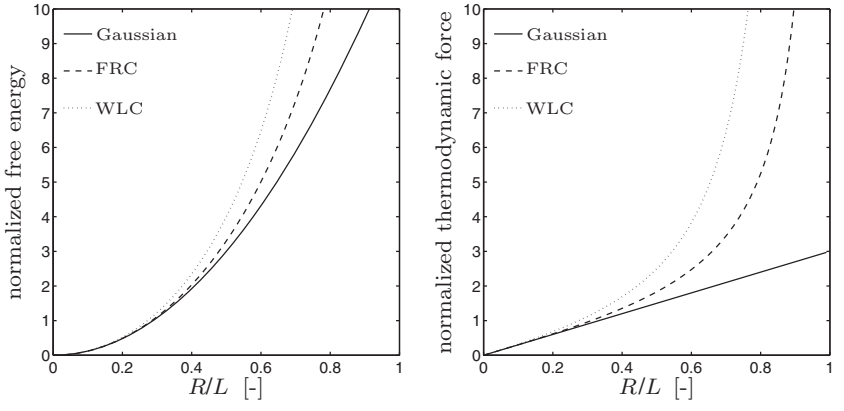

Figure 3. The qualitative plots of the free energy (on the left) and the force (on the right) of a flexible chain according to the Gaussian approximation, the freely rotating chain (FRC) and the worm-like chain (WLC) models. The latter two incorporate finite extensibility and display infinite chain stiffening as the end-to-end distance R approaches the limiting value.

zero value at the zero separation of the chain ends (see Figure 3). This implies that the chain energy as the function of the stretch vector $\psi_f(\boldsymbol{\lambda}) = \psi_f(|\boldsymbol{\lambda}|)$ is strictly convex in $\mathbb{R}^3$, i.e. for any $\boldsymbol{\lambda}_1, \boldsymbol{\lambda}_2 \in \mathbb{R}^3$ and any $\alpha \in [0,1]$

$$\psi_f(|\boldsymbol{\lambda}|) \le \psi_f(\alpha|\boldsymbol{\lambda}_1| + (1-\alpha)|\boldsymbol{\lambda}_2|) \le \alpha\psi_f(|\boldsymbol{\lambda}_1|) + (1-\alpha)\psi_f(|\boldsymbol{\lambda}_2|), \tag{42}$$

where $\boldsymbol{\lambda} = \alpha\boldsymbol{\lambda}_1 + (1-\alpha)\boldsymbol{\lambda}_2$. As long as the energy of a single fibre is convex in $\boldsymbol{\lambda}$ the network total energy Ψ_{net} or equivalently the network average $\langle\psi_f\rangle$ minimized in (32) are also convex with respect to the distribution of stretch in terms of the variable function $\boldsymbol{\lambda}(\boldsymbol{\lambda}_0)$: $S_0 \mapsto \mathbb{R}^3$. Taking into account that the minimized network energy is bounded below by zero and is continuous in $\boldsymbol{\lambda}$ as well as the linearity of the maximal advance path constraint, the solution of the constrained minimization problem (32) exists and is unique unless the objective $\Psi_{\mathrm{net}}[\boldsymbol{\lambda}]$ is undefined in the whole constraint

subspace. This may occur at high macroscopic deformations in networks with infinitely stiffening chains when the network can not deform without violating the limiting extensibility of the filaments. As long as this scenario is avoided, the deformation gradient $\boldsymbol{F}$ belongs to the admissible set $\mathfrak{F}$ that can be shown to be convex and the network responds to it with the equilibrium microstretch $\boldsymbol{\lambda}^*(\boldsymbol{F})$.

Together with the relaxed microdeformation $\boldsymbol{\lambda}^*(\boldsymbol{F})$ the homogenized network free energy (35) is as well defined as a function of the macroscopic strain $\Psi^*_{\text{net}}(\boldsymbol{F})$ for all $\boldsymbol{F}\in\mathfrak{F}$. Furthermore it will be strictly convex in $\boldsymbol{F}$ in the whole domain $\mathfrak{F}$. Indeed, consider two different deformation gradients $\boldsymbol{F}_1, \boldsymbol{F}_2 \in \mathfrak{F}$ and their linear combination $\boldsymbol{F} = \alpha\boldsymbol{F}_1 + (1-\alpha)\boldsymbol{F}_2 \in \mathfrak{F}$ with $\alpha \in [0,1]$. Let $\boldsymbol{\lambda}^*_1$ and $\boldsymbol{\lambda}^*_2$ be the equilibrium microdeformations for $\boldsymbol{F}_1$ and $\boldsymbol{F}_2$, respectively, then their linear combination $\boldsymbol{\lambda} = \alpha\boldsymbol{\lambda}^*_1 + (1-\alpha)\boldsymbol{\lambda}^*_2$ will satisfy the linear micro–macro relation for $\boldsymbol{F}$. Correspondingly, the network energy $\Psi_{\text{net}}[\boldsymbol{\lambda}]$ at this microdeformation will be greater or equal than the minimum $\Psi^*_{\text{net}}(\boldsymbol{F}) = \Psi_{\text{net}}[\boldsymbol{\lambda}^*(\boldsymbol{F})]$. On the other hand, due to (42) it will not exceed the linear combination of $\Psi_{\text{net}}[\boldsymbol{\lambda}^*_1]$ and $\Psi_{\text{net}}[\boldsymbol{\lambda}^*_2]$. As a result, the inequality

$$\Psi^*_{\text{net}}(\boldsymbol{F}) \le \Psi_{\text{net}}[\boldsymbol{\lambda}] \le \alpha\Psi^*_{\text{net}}(\boldsymbol{F}_1) + (1-\alpha)\Psi^*_{\text{net}}(\boldsymbol{F}_2) \tag{43}$$

will always hold. The homogenized network free energy, which is convex in $\boldsymbol{F}$ as obtained for the considered type of fibre response, does not appropriately constitute the elastic behaviour of a solid. The so far considered networks of flexible chains will collapse into a point, since their energy is minimal at zero fibre stretch. In reality the steric repulsions between chains as well as their interaction with the solvent molecules in the case of swelling will counterbalance this tendency so that the material attains a certain finite equilibrium volume [6]. One way to account for this effect is to add a repulsive term to the free energy of single fibres as in [23,24] which shifts the equilibrium stretch of an unloaded fibre to the non-zero value and corresponds to the case considered in the next Subsection 5.2. In reality, the volumetric forces are essentially intramolecular and should not be referred to single fibres and therefore be represented in forms other than (31). To not get beyond the scope of this work, these intramolecular interactions are assumed to have no effect on the network mechanics. They can be associated phenomenologically with the essential incompressibility of the material and introduced by the additional term $\Psi_{\text{vol}}(J)$, where $J = \det \boldsymbol{F}$, accounting for the volumetric deformation in the total free energy of the material given as

$$\Psi(\boldsymbol{F}) = \Psi_{\text{vol}}(J) + \Psi^*_{\text{net}}(\boldsymbol{F}). \tag{44}$$

Such an additive split is commonly adopted for hyperelastic materials. The bulk energy Ψ_{vol} represents a steep convex potential well at the minimum $J=1$ since the steric forces have usually a much greater magnitude compared to the response of flexible chains. These forces are then responsible for the hydrostatic stress contribution resulting from negligible small volume changes. It should be noted that the homogenized free energy given by (44) is a polyconvex function of the deformation gradient, since $\Psi_{\text{vol}}(J)$ is convex in J and $\Psi^*_{\text{net}}(\boldsymbol{F})$ is convex in $\boldsymbol{F}$, and hence constitutes a stable elastic solid [41].

Consider now in particular the case of a network with Gaussian chains. As long as the initial end-to-end distance of the chains is equal to the most probable value $R_0 = \sqrt{N}b$, which is a common assumption [20,22], the free energy can be expressed as $\psi_f = \frac{3}{2}k_B T|\boldsymbol{\lambda}|^2$. The axial stretch conjugate chain force $f_f = 3k_B T|\boldsymbol{\lambda}|$ is then linear in $|\boldsymbol{\lambda}|$, which allows one to solve (34) for the equilibrium stretch vector as

$$3k_B T|\boldsymbol{\lambda}^*|\frac{\boldsymbol{\lambda}^*}{|\boldsymbol{\lambda}^*|} = \boldsymbol{v}\boldsymbol{\lambda}_0 \quad \Leftrightarrow \quad \boldsymbol{\lambda}^* = \frac{\boldsymbol{v}}{3k_B T}\boldsymbol{\lambda}_0. \tag{45}$$

One can see that this microstretch results from an affine transformation of the initial orientations $\boldsymbol{\lambda}_0$ by the map $\boldsymbol{v}/3k_B T$ which can only satisfy the constraint (30) if

$$\langle \boldsymbol{\lambda}^* \otimes \boldsymbol{\lambda}_0 \rangle = \frac{1}{3}\frac{\boldsymbol{v}}{3k_B T} = \frac{1}{3}\boldsymbol{F} \quad \Leftrightarrow \quad \frac{\boldsymbol{v}}{3k_B T} = \boldsymbol{F}. \tag{46}$$

Correspondingly, $\boldsymbol{\lambda}^* = \bar{\boldsymbol{\lambda}} = \boldsymbol{F}\boldsymbol{\lambda}_0$, which implies that the network of Gaussian chains will always deform affinely with the macroscopic strain.

The chain stretch will only redistribute non-affinely if the chain response is substantially non-linear. To illustrate this, the networks composed of non-Gaussian freely rotating chains that possess this property are considered next. For this case the solution to the constrained minimization problem (32) can not be derived in closed form. Therefore the equilibrium network microstretch $\boldsymbol{\lambda}$ and the homogenized stress $\boldsymbol{P}$ are found numerically. Examined are three model networks with chain sizes $N = 4$, 16, 64 and corresponding limiting stretch values $\lambda^{\lim} = \sqrt{N} = 2$, 4, 8. Although the situation of a chain length being equal to only four statistical segments is not well described by the inverse Langevin approximation and is rarely found in real elastomer networks, it is considered here for an illustrative purpose. The proposed model predicts the response of these networks in an essentially different way as the full affine network models [15,28].

Due to the internal relaxation of the microdeformation accounted by the maximal advance path constraint, the non-affine network behaves softer. One can conclude this by the elastic stresses that are produced by the affine and non-affine networks and compared in Figure 4. The nominal stresses are computed taking account of material incompressibility at isochoric uniaxial and equibiaxial tension for the three considered networks. It can be noticed that for the same chain parameters the affine network stiffens at significantly lower strains than the non-affine one. The affinely deformed chains reach the extensibility limit as soon as at least one of the principal stretches approaches $\lambda^{\lim}$. As a result, in both the uniaxial and the equibiaxial tension, the stress goes to infinity when λ_x gets close to 2, 4, 8 depending on the chain length. The non-affine networks predicted by the proposed approach do behave differently. Once the chains that are aligned closely to the direction of tension become highly extended, the stretch in the network is redistributed so that the already highly stretched chains experience lower stretch by means of straining and reorientation of the other chains, which results in a decreasing network total energy.

This redistribution is illustrated in Figures 5 and 6. The former displays the evolution of the maximal absolute stretch value $\lambda^{\max} = \max\{|\boldsymbol{\lambda}(\boldsymbol{\lambda}_0)|,\ \boldsymbol{\lambda}_0 \in S_0\}$ in the three examined networks with the macroscopic deformation for both types of

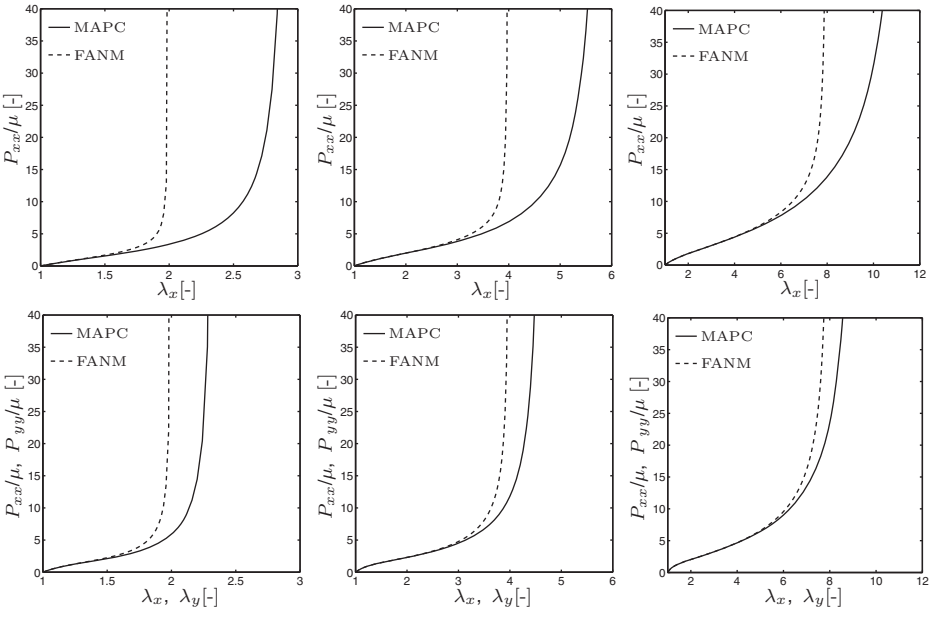

Figure 4. Mechanical stresses predicted by the proposed model (MAPC) and the full affine network model (FANM) for uniaxial tension (top row) and equibiaxial tension (bottom row) of a model incompressible material with unit modulus $\mu = nk_{\mathrm{B}}T = 1$, network functionality $f = 4$ in the MAPC model, and three different values of chain extensibility limit $\sqrt{N} = 2, 4, 8$. The proposed non-affine network response is softer and results in different limiting stretches in uniaxial and equibiaxial loading which is not the case for the affine model.

loading. It can be clearly seen that $\lambda^{\max}$ is smaller than the principal stretch λ_x and reaches the extensibility limit $\lambda^{\lim}$ depicted by dotted horizontal lines for the considered chain lengths $N = 4$, 16, 64 at much higher macroscopic deformations, compared to the affine case. The difference of the stretch at which the affine and the non-affine networks stiffen is significant and is nearly as much as 50% in the case of uniaxial loading. Due to the stretch redistribution the network of chains with limiting extensibility $\lambda^{\lim} = 8$ can attain elongation λ_x up to 11.72. In the case of the equibiaxial deformation the difference is not that profound but still present.

This can be further examined by the example of another model network with chains of length $N = 9$ and extensibility limit $\lambda^{\lim} = 3$. The distribution of the microstretch $\boldsymbol{\lambda}$ of this network at two different macroscopic strains is shown in Figure 6. At both deformations the maximal absolute stretch is close to the limit of 3. However at the uniaxial tension the network is stretched up to $\lambda_x = 4$, which is much larger than the stretch of $\lambda_x = \lambda_y = 3.5$, and the network can undergo equibiaxial tension. When the material is strained in two directions the network paths oriented closely to the plane of the biaxial strain also have to be axially strained due to the reasoning given in Section 3. This imposes much stronger kinematic constraints on the microstretch of the fibres compared to the uniaxial case for which only a relatively small fraction of paths aligned with the principle direction are significantly extended. As a result there is less freedom for the stretch redistribution and it deviates less from the affine distribution, which evidently can be seen in Figure 6.

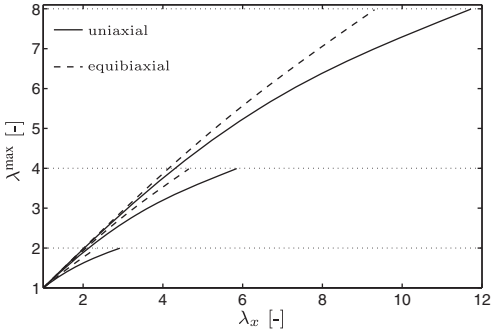

Figure 5. Variation of the maximal absolute value of the microstretch $\lambda^{\max}$ with the increase of the macroscopic strain in the uniaxial and equibiaxial tension predicted by the MAPC model for three networks of functionality $f=4$ composed of chains with different values of extensibility limit $\sqrt{N}=2$, 4, 8 represented by dotted horizontal lines. When $\lambda^{\max}$ approaches this limit the network stiffens as shown in Figure 4.

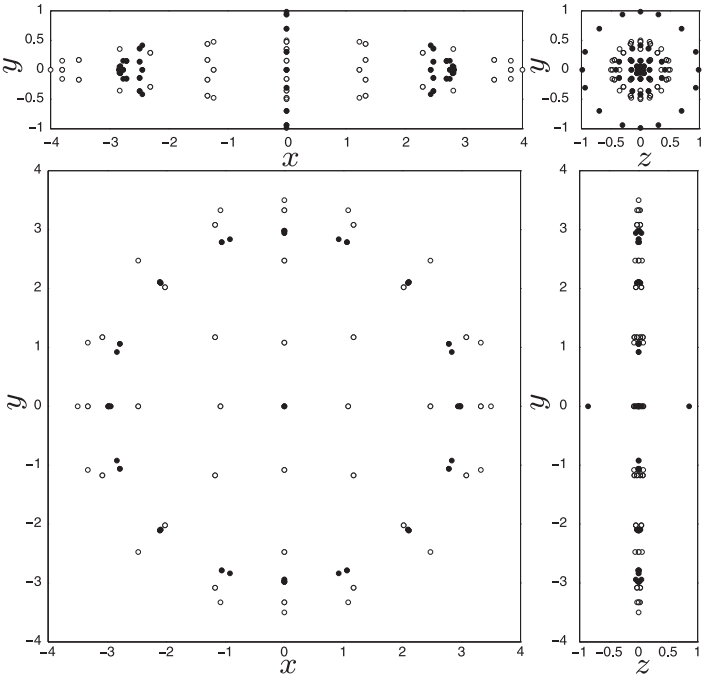

Figure 6. Non-affine microstretch $\boldsymbol{\lambda}^*$ predicted by the MAPC model (filled circles) in a network of chains with extensibility limit $\sqrt{N}=3$ compared to the affine stretch $\bar{\boldsymbol{\lambda}}$ (empty circles) for uniaxial tension with $\lambda_x=4$ (top row) and equibiaxial tension with $\lambda_x=\lambda_y=3.5$ (bottom row). The plotted dots display the end points of the fibre stretch vectors in $x-y$ and $z-y$ plane projections. The fibres have the initial discrete orientations corresponding to the quadrature formula [35] used for the numerical solution.

5.2. *MAPC predicted non-affine deformation in networks of stiff filaments*

In this subsection networks comprised of stiff filaments are considered. These filaments attain a minimum of free energy at an end-to-end distance which is non-zero. Correspondingly, such fibres can support both tensile and compressive axial loadings which is in contrast to the flexible chains considered in the previous Subsection 5.1 which only produce positive thermodynamic forces. This behaviour is typical for *mechanical microscopic fibres* that constitute paper and various non-woven materials [6]. *Semiflexible biopolymers* also belong to the category of stiff filaments. Their mixed entropic/enthalpic response is characterized by an essential anisotropy with respect to tension and compression. The mechanics of semiflexible polymer strands is described by numerous models mainly based on the Kratky–Porod chain representation [39,42–46]. A particular model for semiflexible filaments suggested in [36] and the linear elastic spring model are used for the network simulations presented in this subsection and are briefly summarized in Table 3. The change of free energy and the predicted axial force due to extension of these two models are shown in Figure 7.

What is expected in such a situation is that the three-dimensional networks of the initially undeformed fibres display a stable rigidity with respect to all types of deformation including compression, tension and shear, at least when they are small. A more detailed examination of the networks composed of fibres that only resist to axial straining indicates that their rigidity depends on the network geometry and, in particular, the functionality. Maxwell counting of the degrees of freedom owned by the network junctions and the constraints introduced by the fibres shows that the minimal functionality required for the rigidity is six [12,13,47]. The networks of functionality $f=4$ chosen to illustrate the homogenization approach proposed in this work are therefore unstable, unless reinforced by the elasticity mechanisms supplementary to the axial straining of fibres. In particular instant mechanical bending of filaments may be addressed in this respect as an important factor sustaining the rigidity of the floppy tetrafunctional networks [8,48,49]. The bending is not incorporated into the presented homogenization approach in this work. The non-affine relaxed network microdeformation predicted by the MAPC model can be viewed therefore as an approximation in the limit when the contribution of the stabilizing bending forces is small compared to the axial straining of the fibres.

The non-affine stretch redistribution in the case of stiff tetrafunctional networks is generally shown to be qualitatively different to that of the flexible fibre networks. As illustrated in Figure 7, the free energy ψ_f of stiff fibres is not a convex function of the stretch vector $\boldsymbol{\lambda} \in \mathbb{R}^3$ anymore, although it may be convex in $|\boldsymbol{\lambda}|$ as for the linear spring. In particular, the energy is non-convex when the fibres are in contraction $|\boldsymbol{\lambda}| < 1$ and hence exert negative forces. As a consequence the network will not display a stable behaviour at arbitrary macroscopic strains in contrast to the situation considered in the previous Subsection 5.1. The networks lose stability in a specific manner, namely, fibres only reorient with no axial deformation. Within the statistical description this peculiar microdeformation is defined by a stretch vector that has unit length for all orientations $\boldsymbol{\lambda}_0$, namely

$$|\boldsymbol{\lambda}(\boldsymbol{\lambda}_0)| = 1 \quad \forall\, \boldsymbol{\lambda}_0 \in S_0. \tag{47}$$

Table 3. Stiff filament models.

Model	Free energy ψ_f	Thermodynamic force F_f
Linear spring[a]	$\frac{1}{2}\kappa\frac{(R-R_0)^2}{R_0}$	$\kappa\frac{R-R_0}{R_0}$
Semiflexible chain[b]	$k_{\mathrm{B}}T\frac{\pi^2 l_p}{2L}\left(1-\frac{R^2}{L^2}\right)+\frac{2k_{\mathrm{B}}TL}{\pi l_p}\left(1-\frac{R^2}{L^2}\right)^{-1}$	$k_{\mathrm{B}}T\frac{R}{L^2}\left(\frac{4L}{\pi l_p}\left(1-\frac{R^2}{L^2}\right)^{-2}-\frac{\pi^2 l_p}{L}\right)$

Notes: [a]R_0 is the initial length of a fibre, κ is the axial stiffness; for an elastic bar $R_0 = L$ is the length of the bar, $\kappa = EA$, where E is the elastic modulus and A is the cross-sectional area.
[b]In [36] a force to extension relation in terms of the filament contour length L and the persistence length $l_p = \varkappa/k_{\mathrm{B}}T$ is suggested; $\varkappa$ is the bending stiffness; the filament end-to-end distance R_0 in the unloaded state is defined by $1-(R_0/L)^2 = 2L/(\pi^{3/2}l_p)$.

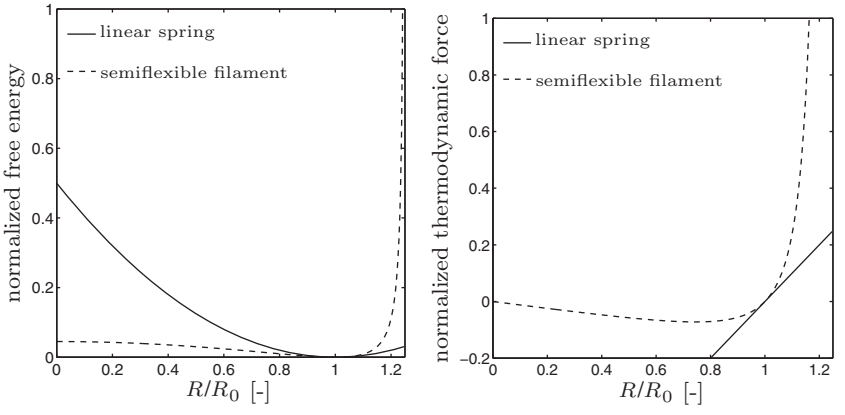

Figure 7. Free energy (on the left) and thermodynamic force (on the right) scaled by the stiffness $\partial^2\psi_f/\partial R^2$ at $R = R_0$ of a linear spring and a semiflexible filament. The latter type of fibres demonstrate anisotropy of the response with respect to tension and compression as well as infinite stiffening when strained up to the full contour length.

In such a state the network attains the minimal possible total energy and produces no mechanical stress, since all the fibre forces are zero. The macroscopic deformations from a set $\bar{\mathfrak{F}} \subset \mathrm{SO}(3)$ at which this yield response is observed can be specifically characterized.

Consider an arbitrary unit microstretch (47) that occurs at some macroscopic deformation with the deformation gradient $\boldsymbol{F}$. The latter can be polar decomposed as $\boldsymbol{F} = \boldsymbol{V}\boldsymbol{R}$, where $\boldsymbol{R}$ is the rotational part of the deformation, and $\boldsymbol{V} = \mathrm{diag}[\lambda_x, \lambda_y, \lambda_z]$ is the stretch part. The maximal advance path constraint (30) gives then the following identity for the macroscopic stretch

$$\langle \boldsymbol{\lambda} \otimes \boldsymbol{R}\boldsymbol{\lambda}_0 \rangle = \frac{1}{3}\boldsymbol{V}. \tag{48}$$

The trace of the left-hand side (48) is equal to $\langle \boldsymbol{\lambda} \cdot \boldsymbol{R}\boldsymbol{\lambda}_0 \rangle$ which does not exceed 1, since both vectors $\boldsymbol{\lambda}$ and $\boldsymbol{R}\boldsymbol{\lambda}_0$ are unit. The trace of the right-hand side satisfies another inequality, namely $\frac{1}{3}\mathrm{tr}\boldsymbol{V} = \frac{1}{3}(\lambda_x + \lambda_y + \lambda_z) \geq (\lambda_x\lambda_y\lambda_z)^{1/3}$, since all the principal stretches are positive. Combining these two observations one can finally deduce that the network can lose stability due to the fibre reorientation if only the macroscopic volumetric deformation is negative. That is, the deformation gradients from $\bar{\mathfrak{F}}$ have a Jacobian smaller than 1, i.e. $J = \det \boldsymbol{F} < 1$. Correspondingly, the admissible set $\mathfrak{F}$ contains at least all the macroscopic deformations for which $J \geq 1$.

The stable response for $\boldsymbol{F} \in \mathfrak{F}$ is produced by the equilibrium microscopic stretch and can uniquely be determined by (34) as

$$\boldsymbol{\lambda}^* = f_f^{-1}(|\boldsymbol{v}\boldsymbol{\lambda}_0|)\frac{\boldsymbol{v}\boldsymbol{\lambda}_0}{|\boldsymbol{v}\boldsymbol{\lambda}_0|}, \tag{49}$$

where the inverse fibre force function f_f^{-1} is well defined and gives for positive $|\boldsymbol{v}\boldsymbol{\lambda}_0|$ an absolute value of stretch

$$|\boldsymbol{\lambda}^*| = f_f^{-1}(|\boldsymbol{v}\boldsymbol{\lambda}_0|) > 1, \tag{50}$$

which is greater than 1 as can be seen in Figure 7. As a consequence, the stable microdeformation of stiff tetrafunctional networks with no other mechanisms like bending, which could support the rigidity, requires that all the fibres constituting it are in tension. Once the stretch in the network approaches a unit value with the change of macroscopic deformation, the network starts folding by means of the abundant kinematic modes, which Maxwell counting predicts in the case of functionality $f = 4$. The transition between the stable network deformation regime at $\boldsymbol{F} \in \mathfrak{F}$ and the floppy reorientation at $\boldsymbol{F} \in \bar{\mathfrak{F}}$ is illustrated in Figure 8. It shows schematically the division of the deformation gradient space SO(3) into a stable and unstable domain.

Furthermore, the two types of the microdeformation discussed above are demonstrated for the example of uniaxial tension considering the network of linear elastic bars with the response outlined in Table 3. When subject to isochoric uniaxial tension $\boldsymbol{F}_1 = \mathrm{diag}[1.4, 0.8452, 0.8452]$ this network will attain a stable equilibrium stretch shown in the top row of Figure 9. In full accordance with (50) at the relaxed state all fibres are elongated. In the situation when fibre forces are positive, the same holds true for the resulting homogenized normal stresses found as $\boldsymbol{P}_1/n\kappa = \mathrm{diag}[0.0412, 0.0180, 0.0180]$. If not constrained in the direction perpendicular to the applied axial strain, this material will tend to contract gradually in the transverse direction, so that the stress components P_{yy}, P_{zz} vanish. This will be only achieved at the macroscopic strain $\boldsymbol{F}_2 = \mathrm{diag}[1.4, 0.5979, 0.5979]$ at which the fibres will become unloaded as shown in the bottom row of Figure 9. This state is at the boundary between the two regions $\mathfrak{F}$ and $\bar{\mathfrak{F}}$. Remarkably the axial stress P_{xx} will also vanish at this point, which means that the network will display no resistance to the uniaxial tension, provided it can shrink freely.

The above demonstrated specific volumetric response is investigated separately. The nearly 50% shrinking predicted by the MAPC model for the network of elastic fibres is not typical, for most materials show a volumetric expansion when axially strained. The affine network models do not capture this specific shrinkage

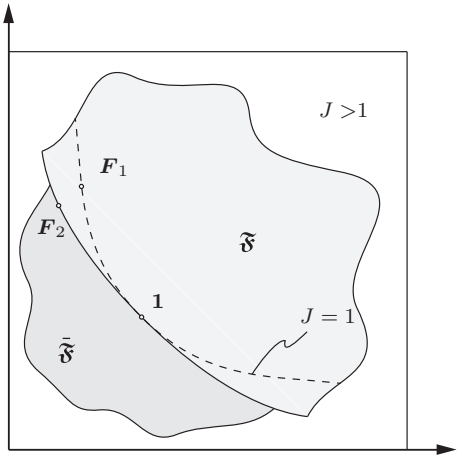

Figure 8. Schematic representation of the deformation gradient space SO(3) and its partition into the domain $\mathfrak{F}$ for which networks display a stable equilibrium response and the domain $\bar{\mathfrak{F}}$ where the networks lose stability by fibre reorientation together with the isochoric deformation $\boldsymbol{F}_1$ from $\mathfrak{F}$ and the deformation $\boldsymbol{F}_2$ with negative volumetric change located on the boundary between $\bar{\mathfrak{F}}$ and $\mathfrak{F}$.

effect. The same network as considered above but deformed affinely produces at the isochoric macroscopic strain $\boldsymbol{F}_1$ the homogenized stress $\boldsymbol{P}_{\text{affine}}/n\kappa = \text{diag}[0.0723, -0.0123, -0.0123]$ which is negative in the transverse direction, in which the fibres will be compressed. Correspondingly, such a network will expand transversely and the volume will increase if the material is only loaded in the axial direction.

As shown above, the maximal advance path constraint model predicts a non-trivial non-affine deformation for networks with fibres that produce forces simply linear in extension. One can expect an even more peculiar behaviour in the case of semiflexible filaments which display essentially non-linear stiffening as outlined in Figure 7. This in particular is illustrated by the following example of a model semiflexible network subject to the macroscopic shear $\boldsymbol{F} = \boldsymbol{1} + \gamma_{xy}\boldsymbol{e}_x \otimes \boldsymbol{e}_y$, where $\boldsymbol{e}_x$ and $\boldsymbol{e}_y$ are two basis vectors of a Cartesian coordinate system. This deformation is isochoric and therefore (as shown above) the equilibrium microdeformation exists and is stable, unless the shear γ_{xy} is too high so that the filaments reach the limiting extensibility. The test parameter set for the semiflexible fibres described by the model outlined in Table 3 is chosen so that the unloaded fibres have the initial end-to-end distance close to the contour length $R_0 = 0.9L$. Correspondingly, the limiting stretch value is as large as $\lambda^{\lim} = 1.11$. The mechanical response of this network predicted by the MAPC model and the full affine network model is presented in Figure 10 for the two components of the Piola–Kirchhoff stress tensor, the shear stress P_{xy} and the normal stress P_{yy}, that define the traction on the horizontal surface where the shear deformation is applied. Just as in the case of flexible chains with limiting extensibility, the non-affine redistribution allows the network to undergo much larger strains. If in the affine case the fibres aligned initially at 45° with respect to the shear direction reach the extensibility limit $\lambda^{\lim} = 1.11$ at $\gamma_{xy} = 0.2121$, the non-affine network described by the proposed MAPC model can be sheared up to $\gamma_{xy} = 0.5$ and

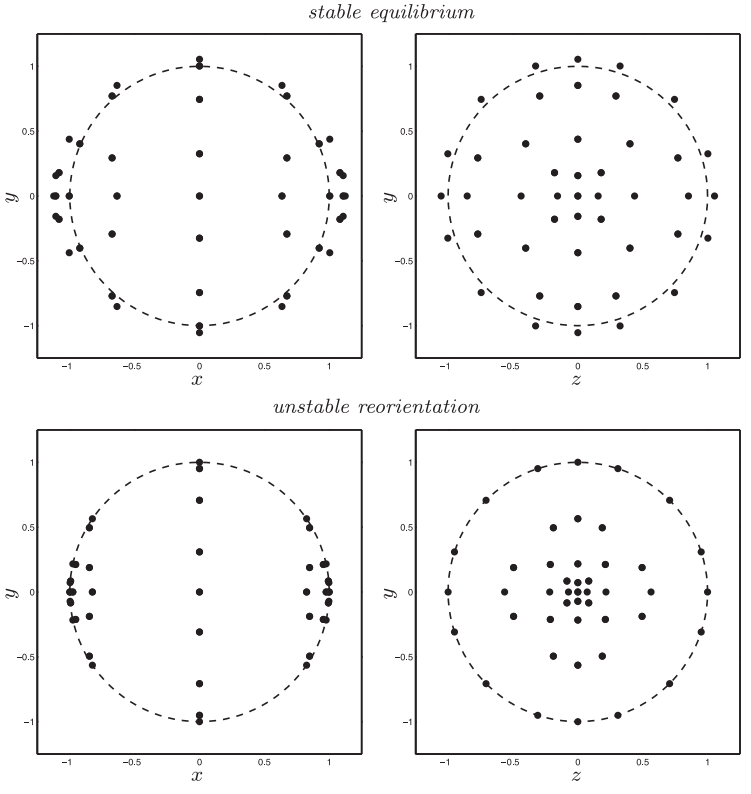

Figure 9. Illustration of the two types of microdeformation in stiff tetrafunctional networks of linear springs predicted by the MAPC model. The stable equilibrium microstretch of the network attained at isochoric uniaxial strain $\boldsymbol{F}_1$ (top row) and the acquisition of unit stretch in the network with the loss of rigidity after the shrinkage in the transverse direction at strain $\boldsymbol{F}_2$ (bottom row). The same graphical representation of the microstretch as in Figure 6 is used. The unit dashed circle is plotted to assist the identification of elongated fibres in the first case and reoriented fibres with the unit stretch in the second case.

beyond. The microstretch in the network at this macroscopic deformation is shown in Figure 11. The fibres at this equilibrium state of the network are all in tension. The magnitude of fibre stretch, remarkably, displays very small variations from $|\boldsymbol{\lambda}^*| = 1.0443$ to $|\boldsymbol{\lambda}^*| = 1.0603$ that can hardly be seen in the figure, unlike the affine deformation for which the stretch alters from compression $|\bar{\boldsymbol{\lambda}}| = 0.7906$ to tension $|\bar{\boldsymbol{\lambda}}| = 1.2748$.

Finally, two other interesting features of the non-affine network, which are not related to the stiffening of the considered semiflexible filaments and concern the response at small and moderate deformations, are investigated. Firstly, the magnitude of the value for the normal stress P_{yy} appears to be higher than the value of the shear stress P_{xy}. Neither the affine network, in particular, nor conventional solid materials, in general, display such a behaviour at an applied shear deformation. Recent experimental investigations of biopolymer gels report though a similar atypical normal stress response of the magnitudes that substantially exceed

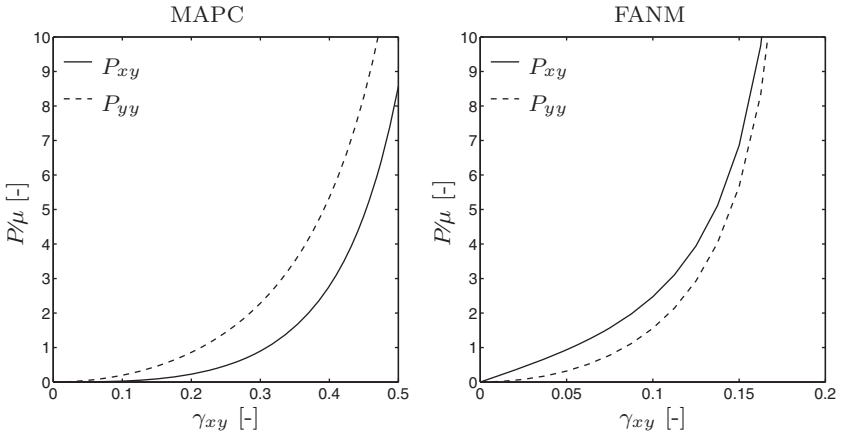

Figure 10. Dimensionless mechanical stresses of network made of semiflexible filaments predicted by the MAPC model (on the left) and the full affine network model (on the right) for macroscopic shear with $\gamma_{xy} = 0.5$. The shear stress P_{xy} and the normal stress P_{yy} are scaled by the characteristic modulus $\mu = nk_{\mathrm{B}}T$.

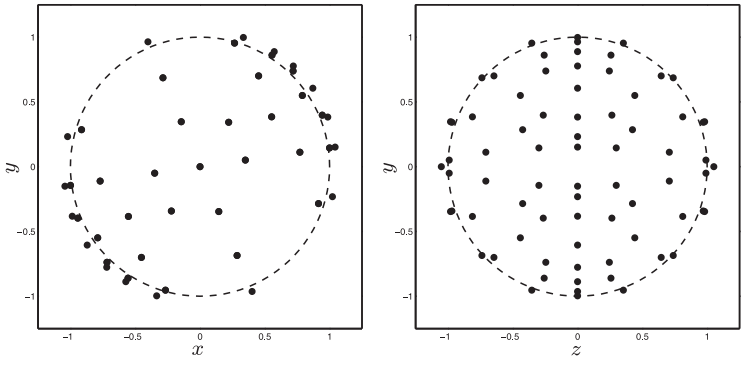

Figure 11. Microstretch at an applied shear deformation in a network made of semiflexible filaments. The same graphical representation of the microstretch as in Figure 6 is used. The unit dashed circled is plotted to demonstrate that all the fibres are elongated as stated in (50) for the stable equilibrium microdeformation.

the values of the shear stress [50,51]. The non-affine redistribution of filament stretch in the network gives an adequate qualitative explanation of this phenomenon. The second feature of the response predicted by the MAPC is the scaling of the stresses with small values of shear strain. For conventional materials the shear stress displays a linear proportionality $P_{xy} \sim \gamma_{xy}$ when γ_{xy} is close to zero, whereas the normal stress scales with the square of shear $P_{yy} \sim \gamma_{xy}^2$. This regularity is also valid for the homogenized response of the affine network (see Figure 10). The non-affine network, on the contrary, produces mechanical stresses that scale as $P_{xy} \sim \gamma_{xy}^3$ and $P_{yy} \sim \gamma_{xy}^2$, which again demonstrates that the shear stress response is softer than the normal stress. The network displays zero stiffness in the initial undeformed state when all the fibres are not stretched and, therefore, does not resist to shear at $\gamma_{xy} = 0$.

6. Conclusion

This work explores the mechanics of materials with random network microstructures. It presents a new kinematic constraint relating the microscopic deformation of fibres to the macroscopic strain of the continuous solid that results in an efficient homogenization of the elastic response produced by these soft materials. This relation is established with the help of a special statistical description of the network microdeformation that provides extensive information about the reorientation and axial straining of the fibres. The design of the constraint is based on kinematics of maximal advance paths, which allows for a robust transition from the microscopic scales of the network to macroscopic scales of the deformed material. The maximal advance path constraint imposes restrictions not on the stretch of a single fibre but on the microdeformation of the network as a whole. Furthermore it includes important topological characteristics of the network like the functionality of the junctions. Remarkably, for the case of tetrafunctional networks the constraint takes a compact tensorial form which can be clearly interpreted. It is shown that the exact distribution of the variable microscopic stretch defined by this network model can be determined by the principle of minimum averaged free energy, which ultimately leads to the derivation of the homogenized elastic response of the relaxed network at equilibrium. The predicted equilibrium microstretch is non-trivially distributed and depends on the particular response of the chains. The qualitative difference of the microdeformation and the homogenized stress response is shown for tetrafunctional networks with two different types of fibres, namely, flexible chains and stiff filaments.

In the former case, the networks are shown to undergo an essential non-affine deformation when their fibres approach their finite extensibility. This gives a consistent explanation for the difference in the stiffening of elastomers at uniaxial and equibiaxial extension which is well known since the first publication of the experimental data for vulcanized rubber in [19]. In this respect the model supports the justification of other non-affine models like the 8-chain model [22] and the non-affine microsphere model [20] which both suggest a redistribution of chain stretch in the polymer networks. Moreover, in agreement with the latter model this non-affine deformation is associated with the relaxation of the network by the internal degrees of freedom.

A very peculiar behaviour is also predicted for networks composed of stiff filaments. The microscopic stretch is shown to be non-affine not only at larger macroscopic strains when the fibres get highly elongated but also at small strains. Furthermore, one can identify a specific soft regime in which the network deforms solely by reorientation without axial straining of the stiff fibres and therefore produces no mechanical response. The transition from this unstable regime to the stable equilibrium behaviour results in a particular scaling of shear and normal stresses obtained for simple shear loading and represents a limiting case. As argued above, the stretch of fibres in the real semiflexible networks is stabilized by bending. The response of stiff filaments to bending is commonly much smaller than their response to axial straining. Nevertheless, in the situation when fibre axial forces become zero, which is the case for the fibre reorientation in the predicted unstable regime, bending can become the dominant mechanism of network elasticity. Instead

of the loss of rigidity by the network in the undeformed state as demonstrated in this work, a soft but stable elastic response of the material supported by filament bending as reported in [9–11,21] is expected.

The presented homogenization scheme is universally applicable to the materials with random network microstructures formed by fibres of different nature. The use of the maximal advance path constraint is especially justified in cases when the microscopic deformation significantly deviates from the affine stretch, for it effectively captures on average the complex kinematics of connected fibres. Furthermore, the proposed model provides a broad framework for future extensions. For flexible chains, the model gives a very realistic picture of the network microdeformation. Nevertheless, the elastic properties of real elastomers can not be described in terms of the conformational statistics of single chains only. Thermal fluctuations of the junction points [52,53] and interaction of chains over their length [54–57] play an essential role and have a corresponding energetic contribution. The incorporation of these factors into the developed description of the network micromechanics reaches far beyond the illustrative objectives of this work and is a subject for future extensions. For stiff filaments, the proposed maximal advance path constraint model is valid for the stretching-dominated regime. The incorporation of the instant bending of fibres into the proposed model will allow one to capture the response of the stiff networks in the whole range of macroscopic deformations.

The approach proposed in this work provides two main contributions to the mechanics of soft materials. Firstly, it constitutes a universal framework for the development of computational models that can be utilized for the finite element analysis. It is not overly complex and at the same time is quite flexible and suitable for different types of networks. Secondly, the approach has an essential micromechanical justification. As a consequence, it allows one not only to obtain averaged mechanical properties of the material but also to explain how particularly they originate at the microstructure level. Besides the values of the macroscopic quantities such as mechanical stress, the resulting models are capable of predicting by which microscopic forces and which deformed microscopic fibres it is created. This information is crucial for the understanding of elasticity as discussed in this work, as well as other phenomena in soft materials with random network microstructure. In particular, the knowledge of the microstretch distribution gives the key to the failure of such materials and its modelling in the context of the advanced finite element techniques such as those in [58–60].

Acknowledgements

Financial support for this research was provided by the 'Juniorprofessorprogramm des Landes Baden-Württemberg' and the German Research Foundation (DFG) within the Cluster of Excellence in Simulation Technology (ExC 310/1) at the University of Stuttgart. This support is gratefully acknowledged.

References

[1] L.R.G. Treloar, *The Physics of Rubber Elasticity*, 3rd ed., Clarendon Press, Oxford, 1975.
[2] H. Lodish, *Molecular Cell Biology*, W. H. Freeman & Company, New York, 2000.

[3] D. Boal, *Mechanics of the Cell*, Cambridge University Press, Cambridge, 2002.
[4] G. Holzapfel and R. Ogden, *Mechanics of Biological Tissue*, Springer, Berlin, 2006.
[5] J. Hearle, J. Thwaites and J. Amirbayat, *Mechanics of Flexible Fibre Assemblies*, NATO Advanced Study Institutes Series: Applied Sciences, Sijthoff & Noordhoff, Alphen aan den Rijn, 1980.
[6] R. Picu, Soft Matter 7 (2011) p.6768.
[7] L. Gibson, M. Ashby and B. Harley, *Cellular Materials in Nature and Medicine*, Cambridge University Press, Cambridge, 2010.
[8] J. Wilhelm and E. Frey, Phys. Rev. Lett. 91 (2003) Article ID 108103(4).
[9] E. Huisman, C. Storm and G. Barkema, Phys. Rev. E 78 (2008) Article ID 051801(11).
[10] T. van Dillen, P. Onck and E. van der Giessen, J. Mech. Phys. Solids 56 (2008) p.2240.
[11] P. Onck, T. Koeman, T. van Dillen and E. van der Giessen, Phys. Rev. Lett. 95 (2005) Article ID 178102(4).
[12] E. Huisman and T. Lubensky, Phys. Rev. Lett. 106 (2011) Article ID 088301(4).
[13] J. Blundell and E. Terentjev, Proc. R. Soc. A 467 (2011) p.2330.
[14] W. Kuhn and F. Grün, Colloid. Polym. Sci. 101 (1942) p.248.
[15] L.R.G. Treloar and G. Riding, Proc. R. Soc. London, Ser. A 369 (1979) p.261.
[16] C. Storm, J. Pastore, F. MacKintosh, T. Lubensky and P. Janmey, Nature 435 (2005) p.191.
[17] J. Blundell and E. Terentjev, arXiv:0808.4088v1[cond-mat.soft] (2008) p.1.
[18] G. Marckmann and E. Verron, Rubber Chem. Technol. 79 (2006) p.835.
[19] L.R.G. Treloar, Trans. Faraday Soc. 40 (1944) p.59.
[20] C. Miehe, S. Göktepe and F. Lulei, J. Mech. Phys. Solids 52 (2004) p.2617.
[21] C. Heussinger, B. Schaefer and E. Frey, Phys. Rev. E 76 (2007) Article ID 031906(12).
[22] E.M. Arruda and M.C. Boyce, J. Mech. Phys. Solids 41 (1993) p.389.
[23] E. Kuhl, K. Garikipati, E. Arruda and K. Grosh, J. Mech. Phys. Solids 53 (2005) p.1552.
[24] E. Kuhl, A. Menzel and K. Garikipati, Phil. Mag. 86 (2006) p.3241.
[25] J. Palmer and M. Boyce, Acta Biomater. 4 (2008) p.597.
[26] G. Glatting, R.G. Winkler and P. Reineker, J. Chem. Phys. 101 (1994) p.2532.
[27] M. Kroon, Mech. Mater. 42 (2010) p.873.
[28] P. Wu and E. van der Giessen, J. Mech. Phys. Solids 41 (1993) p.427.
[29] V. Alastrué, P. Sáez, M.A. Martínez and M. Doblaré, Mech. Res. Commun. 37 (2010) p.700.
[30] C. Linder, M. Tkachuk and C. Miehe, J. Mech. Phys. Solids 59 (2011) p.2134.
[31] A. Menzel and T. Waffenschmidt, Phil. Trans. R. Soc. Lond. A 367 (2009) p.3499.
[32] P. Flory, *Statistical Mechanics of Chain Molecules*, Hanser Publishers, Munich, 1988.
[33] B. Coleman and W. Noll, Rev. Mod. Phys. 33 (1961) p.239.
[34] M. Doi and S. Edwards, *The Theory of Polymer Dynamics*, Clarendon Press, Oxford, 1986.
[35] Z.P. Bažant and B.H. Oh, Z. Angew. Math. Mech. 66 (1986) p.37.
[36] J. Blundell and E. Terentjev, Macromolecules 42 (2009) p.5388.
[37] W. Kuhn, Colloid. Polym. Sci. 68 (1934) p.2.
[38] E. Guth and H. Mark, Monatsh. Chem. 65 (1934) p.93.
[39] O. Kratky and G. Porod, Recl. Trav. Chim. Pays-Bas 68 (1949) p.1106.
[40] J. Marko and E. Siggia, Macromolecules 28 (1995) p.8759.
[41] M. Šilhavý, *The Mechanics and Thermodynamics of Continuous Media*, Texts and Monographs in Physics, Springer, Berlin, 1997.
[42] M. Otto, J. Eckert and T. Vilgis, Macromol. Theory Simul. 3 (1994) p.543.
[43] F. MacKintosh, J. Käs and P. Janmey, Phys. Rev. Lett. 75 (1995) p.4425.
[44] J. Wilhelm and E. Frey, Phys. Rev. Lett. 77 (1996) p.2581.
[45] R. Winkler, J. Chem. Phys. 118 (2003) p.2919.

[46] J. Blundell and E. Terentjev, J. Phys. A: Math. Theor. 40 (2007) p.10951.
[47] M. Kellomäki, J. Aström and J. Timonen, Phys. Rev. Lett. 77 (1996) p.2730.
[48] D. Head, A. Levine and F. MacKintosh, Phys. Rev. Lett. 91 (2003) Article ID 108102(4).
[49] D. Head, A. Levine and F. MacKintosh, Phys. Rev. E 68 (2003) Article ID 061907(15).
[50] P. Janmey, M. McCormick, S. Rammensee, J. Leight, P. Georges and F. MacKintosh, Nat. Mater. 6 (2007) p.48.
[51] E. Conti and F. MacKintosh, Phys. Rev. Lett. 102 (2009) Article ID 088102.
[52] P.J. Flory, Br. Polym. J. 17 (1985) p.96.
[53] H. James and E. Guth, J. Chem. Phys. 15 (1947) p.669.
[54] R. Deam and S. Edwards, Phil. Trans. R. Soc. Lond. A 280 (1976) p.317.
[55] G. Heinrich and E. Straube, Acta Polym. 34 (1983) p.589.
[56] S. Edwards and T. Vilgis, Rep. Prog. Phys. 51 (1988) p.243.
[57] G. Heinrich and M. Kaliske, Comput. Theor. Polym. Sci. 7 (1997) p.227.
[58] C. Linder and F. Armero, Int. J. Numer. Methods Eng. 72 (2007) p.1391.
[59] F. Armero and C. Linder, Comput. Methods Appl. Mech. Eng. 197 (2008) p.3138.
[60] C. Linder, D. Rosato and C. Miehe, Comput. Methods Appl. Mech. Eng. 200 (2011) p.141.